Fluid dynamics of Antarctic subglacial lakes

by

Nandaha Joseph

M2 internship presented for the degree of Master of science in ocean, atmosphere and climate science (SOAC)

Department of Physics
Université Claude Bernard Lyon 1
Lyon, France

Supervisor: Dr. Louis-Alexandre Couston
University Tutor: Prof. Richard Perkins

September 1, 2021

Abstract

The vertical and horizontal convection in a rectangular domain of aspect ratio 4 with subglacial lakes' boundary conditions is studied using spectral element methods employed in Nek5000. Simulations are performed with a fixed Prandtl number Pr = 1, Ra in the range $10^5 - 10^9$ and horizontal temperature gradient (hg) values in dimensionless form between 0 and 1.0 inclusive. Vertical convection due to geothermal heating at the bottom of the lake dominates at hg values below 0.01 and horizontal convection due to a horizontal temperature gradient at the top boundary dominates for hg values greater than 0.01. Heat flux is positive where the top temperature is coldest that is to say where the ice slab would be thickest and melting. Where as heat flux is negative where the top temperature is warmest and that is where the ice slab would be thinnest and freezing. The scaling laws for Reynold's number, Re, Equilibrium temperature, Te, temperature gradient at the top also called flux and Nusselt number, Nu as function of Ra are respectively deduced as; $Re \sim 0.2Ra^{\frac{3}{11}}$, $T_e \sim 38.5Ra^{-\frac{7}{50}}$, $|F|_{top} \sim 0.3Ra^{\frac{1}{5}}$ and $Nu \sim 0.5Ra^{\frac{1}{6}}$.

Key words: Subglacial lakes, horizontal convection, vertical convection.

Common abbreviations
hg - Horizontal temperature gradient (dimensionless variable)
hc - Horizontal convection
Ke - Kinetic energy
Ra - Rayleigh number
Nu - Nusselt number
RBC - Rayleigh Bernard convection
Re - Reynold's number
Te - Equilibrium temperature

Contents

List of Figures

List of Tables

Acknowledgement

Dedication

The work of this research internship is dedicated to my family and my motherland the republic of Uganda, "For God and my country"

1   Introduction

Antarctica is an ice-covered land mass region located at the south pole of planet earth. It is known to be uninhabited, with very low ice temperatures. This region is covered with thick kilometres of ice about 3-5km[1][2]. Below these thick sheets of ice, there exists some water bodies and these water bodies are the famous subglacial lakes. Subglacial lakes are also believed to exist in Greenland[3] since this region is also covered by ice sheets similar to Antarctica. Subglacial lakes in general are water bodies trapped between thick kilometres of ice sheets and the continental bedrock[1]. The fact that they are located below thick ice sheets, these water bodies are characterised by very high pressures and very low temperatures[4]. Subglacial lakes were discovered using data records of airborne radio echo sounding and seismic sounding of 1970s[1]. Seismic soundings used acoustic waves whereas radio-echo soundings used electromagnetic waves. Radars on vehicles and planes where directed towards the ice sheets and all these were used to gather information on the internal layer of the ice sheets. By looking at the back reflected signals of radio waves or seismic soundings from the internal layering, scientists discovered that some signals were reflected differently depending on the interface/boundary of reflection. The data looked different and showed some kind of differences in the internal layers of ice sheets. The existence of a bright reflection along a horizontal line at depths is what prompted scientists to think that there were subglacial water bodies. Thus Antarctic subglacial lakes and other subglacial lakes in Greenland were discovered in this way. Following this discovery, about about 400 subglacial lakes have been identified in Antarctica[2] and about 50 in Greenland[3]. Figure 1 demonstrates how Lake Vostok (the largest subglacial lake) and other Antarctic subglacial lakes were detected from airborne radio-echo sounding of 1970s[1][5][6]. These subglacial lakes can be classified as stable or unstable subglacial lakes depending on the interaction with the external environment[4]. Stable subglacial lakes are ones which are completely isolated from the earth's climate, they stand alone and they do not exchange their waters with the external water bodies (lakes, rivers or oceans). On the other hand, unstable subglacial lakes are those that are hydrologically active, that is they are connected through networks of subglacial channels and communicate via filling and discharge with the surrounding ocean[4][7]. In this study, we will only focus on the stable subglacial lakes. They are not connected to the external environment and oceans which makes them unique from lakes and oceans that are commonly studied by oceanographers.

Having seen that stable subglacial lakes are completely isolated from the earth's climate and given the thickness of the ice sheets, it follows that unlike other water bodies, subglacial lakes have no light implying that photosynthesis is not possible in these lakes, So we will be interested in knowing how do micro organisms (which may exist in lake Vostok, based on accreted ice analysis [8][1]) survive in these environments. There is no wind and no solar radiation in these lakes so we are also interested in knowing what drives the dynamics (movement of water in these lakes) if they do really exist. Very little information is known about the dynamics of these subglacial lakes. Knowing how microorganisms survive in these environments opens doors to understanding life on extra terrestrial icy moons which are said to have some kind of water packets below the icy crust[9][4]. In this study we try to apply fluid dynamics to subglacial lakes to get some kind of insights of the parameters that control the dynamics of these lakes. Basically we use numerical simulations to model a subglacial lake and study its dynamics. With expeditions to subglacial lakes anticipated in the near future, we find it necessary to try to model a subglacial lake, apply fluid dynamics results and find some variables that can give us a hint on the dynamics of these lakes. If we find variables that can help explain how the flow behaves in these lakes, this can be a starting point to scientists interested in exploring these subglacial lakes. That is one of the motivations of this study. We expect these expeditions to come up with a lot of information and results about subglacial lakes and this will open discussions in comparison to what we would have obtained as our results.

Knowing that there exist no light (or solar radiations) and no winds in these subglacial lakes, we are curious about what could ignite motion of water in these subglacial lakes to favour life of living organisms. One of the first mechanisms thought to bring about dynamics in subglacial lakes is the geothermal heat flux coming from the inside of the earth. This geothermal flux is due to the heat
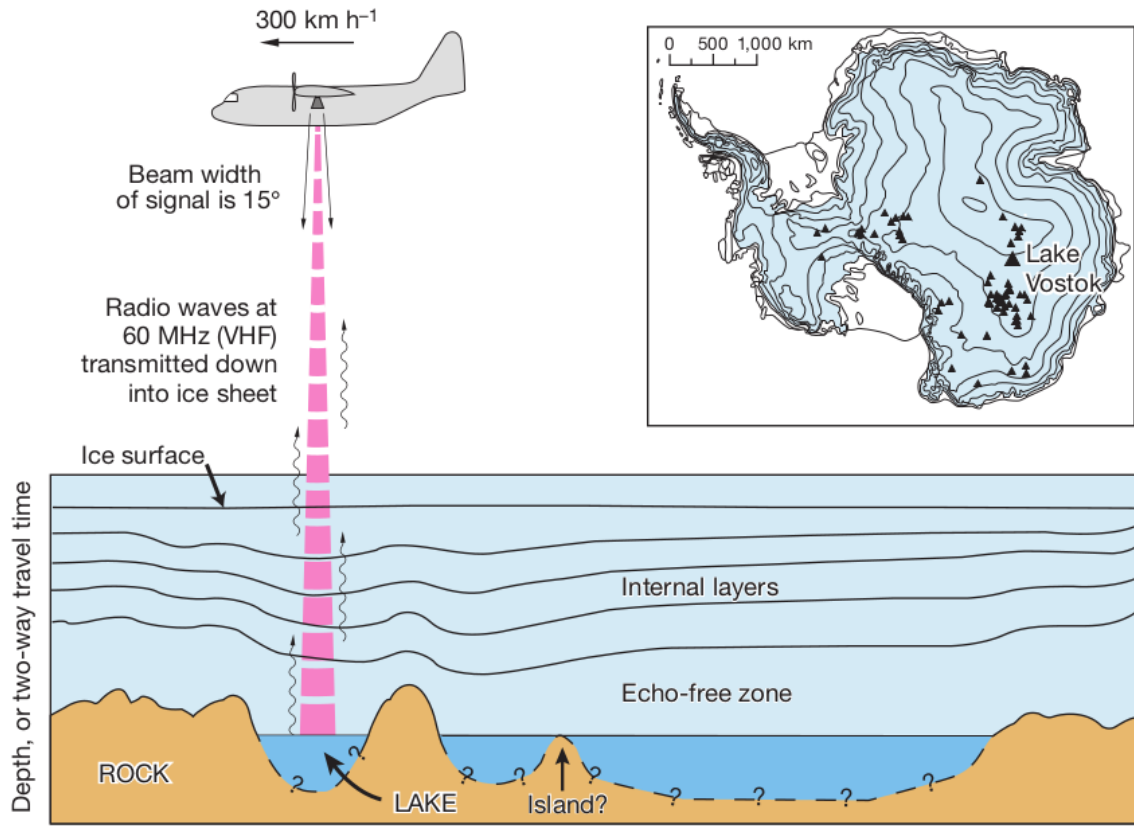
Figure 1: Discovery of Lake Vostok and other Antarctic subglacial lakes using airborne radio-echo sounding records of 1970s. Figure obtained from [1]

produced by the earth's interior that was stored during the formation of planet earth. Due to high compression in the inner core during its formation, a lot of heat was generated and not all the heat generated was radiated outwards, so there still exist some heat coming from the earth's interior to the outer parts of the planet. This heat energy is what contributes geothermal flux. Also, since the bottom part of these subglacial lakes rests on the bedrock, this bedrock contains some radioactive elements that are undergoing radio-activity thus produce some heat energy during the process. These two phenomena contribute a heat flux at the surface of planet earth (subglacial lake bedrock). This geothermal flux is roughly of orders of magnitude $50mWm^{-2}$[8]. This geothermal flux is large enough to trigger flows in subglacial lakes, and these flows can be vigorous enough to suspend micro organisms and nutrients in subglacial lakes[8]. With this geothermal flux heating at the bottom of subglacial lakes, we expect to have Rayleigh Bernard Convection (RBC). RBC is the buoyancy-driven flow of a fluid heated from below and cooled from above. This model of thermal convection was first studied by Henri Bénard in 1900 and Lord Rayleigh in 1916. Since then this topic attained attention and became a canonical fluid dynamics problem with many studies conducted related to RBC. In a subglacial lake, if we have heating from bottom due to geothermal flux, the water masses at the bottom of the lake become warm and less dense and therefore would want to rise. On a contrary the water masses at the top close to the ice-water boundary are cold (because they have to be at the freezing temperature where they are in contact with ice) and dense, therefore would prefer to sink. If the heating is small, the temperature difference may not be sufficient enough to drive any fluid motion and in this case we will have thermal diffusion. However, If the heating is large enough which is the case of the geothermal

heating, there is so much potential energy due to the light water at the bottom and heavy water at the top, that the two water masses can overcome dissipative effects and move, yielding an overturning motion and thus mixing of water in a subglacial lake. In this case we have a Buoyancy-driven convection. The amount of heating required to trigger this Buoyancy-driven convection is controlled by the Rayleigh number(Ra) which is a function of the temperature gradient and the lake's depth cubed. Therefore the Rayleigh number and lake depth are some of control parameters that we need to be aware of when performing our simulations.

The second factor that is thought of to cause motion of water in subglacial lakes is the horizontal temperature difference along the ice-water interface of subglacial lakes[4]. The ice ceiling of subglacial lakes is tilted with angles of tilt in the range 0-0.01 [4] [8] [10] and this causes a pressure difference between the opposite sides of ice-water interface ,i.e., the side with a thick ice slab has a greater pressure than the side with the shallow ice slab. Due to the dependence of melting temperature of ice on pressure[11], a horizontal temperature difference is induced at the tilted ice ceiling of subglacial lakes[11][4]. Therefore the side with a thick ice slab has a low melting temperature compared to the opposite end with a slightly thinner ice slab. A horizontal temperature difference in the fluid drives a horizontal convection leading to motion and overturning of the fluid column [12] [13]. Several studies have been conducted through experiments and(or) simulations and have all revealed that when there is a horizontal temperature difference between two opposite horizontal ends of a fluid, then horizontal convection takes place in the fluid leading to turning of the fluid [14] [15] [16]. This horizontal temperature difference at the tilted ice-water ceiling is large enough to produce horizontal convection in subglacial lakes [8].

We now have an idea that motion of water in subglacial lakes is driven by two processes; one due to geothermal heating leading to a vertical convection controlled by the Rayleigh number (Ra) and secondly horizontal convection due to a horizontal temperature gradient induced at the top of the lake by the tilted ceiling. A competition between these two convections is expected and our aim will be to study the two processes and identify which one of the two dominate and at what scales. The main objective of this study is to perform numerical simulations of both vertical convection and horizontal convection and be able to identify the transition from one form of convection to the other. Also to compute some physical parameters like Nusselt number, Reynolds number and boundary flux that can help us better characterise our system. We should be able to extract the best-fit power law for these parameters for some values of Rayleigh number. The results of this study are discussed in the results and discussion section.

2   Formulation of the problem

2.1   Problem setup

We consider a subglacial lake laying between a thick sheet of ice about 3-5km (which is the typical thickeness of Antarctic ice on top of antarctic subglacial lakes [2]) and the continental bedrock below the lake. In this case we study a stable sublaglacial lake, i.e., one that is completely isolated from earth's climate and oceans, and thus does not communicate with the surrounding earth oceans. It is for this reason that we assume no heat exchanges on the sides of the lake (no flux on the sides). The only flux in the sublacial waters is coming from the bottom of the lake due to geothermal heating from the continental bedrock. The flux due to geothermal flux at the bottom of the lake is denoted by letter F in red in figure 2. We assume a lake of depth, H and length, L such that the aspect ratio, A is given by $A = \frac{L}{H}$. Figure 2 shows a general schematic of a stable subglacial lake.

The interesting feature about most subglacial lakes is the tilted ice roof. Tilted ice roof implies the pressure at the top of the lake is not uniform and this has an influence on the temperature due the freezing temperature dependence on pressure. If H_i^* is the thickness of ice on the left hand side of
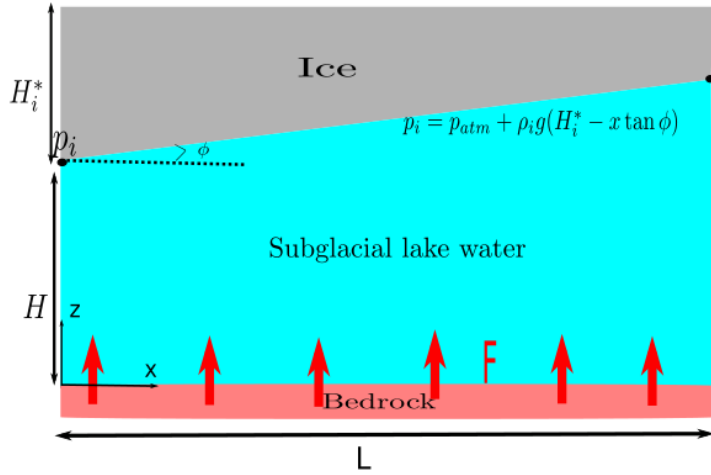
Figure 2: Schematic representation of a subglacial lake with a tilted ice roof, resting on a bedrock. F is the flux from the bedrock due to geothermal heating.

the lake(thicker end), then the ice overburden pressure is given by $P_i = P_{atm} + H_i^* \rho_i g$ where p_{atm} is the atmospheric pressure exerted on the surface of ice sheet, ρ_i is the density of ice. Since H_i^* varies from the left to the right of the domain, the ice overburden pressure is a function of x such that P_i is given by equation 2.1

$$p_i(x) = p_{atm} + \rho_i g(H_i^* - x \tan \phi) \tag{2.1}$$

From equation 2.1, we can see that the pressure on the left is greater than the pressure on the right and thus ice on the left melts very fast with a small value of temperature. Therefore the temperature of the top left is always lower than the temperature on the top right and this brings about a horizontal temperature difference at the top of the subglacial lake. ϕ is the ice tilt angle, these angles are small of magnitudes in range $(0 - 0.01)$[8][10] but they are sufficient enough to induce a horizontal temperature difference at the top of the lake. We consider a two dimension domain thus x and z are the two dimensional coordinates with z the depth of the lake and x, the lake's length.

Figure 3 shows a simplified schematic of a subglacial lake that we have used in building our simulations. For simplicity we assume a flat top surface with the effect of the ice tilted roof represented by the temperature difference (δT) between the top right and top left of the lake. Since we are looking at the case of a stable subglacial lake, we impose no flux on the boundaries. The big red crosses on the sides of figure 3 implies no flux on the sides. The flux at the bottom of the lake due to geothermal heating from the continental bedrock is represented by the red arrows at the bottom of the lake and with letter F. We consider a lake domain of depth H such that z ranges from 0 at the bottom to H at the top. The length of the lake used in this study is 4 such that x ranges from ^-2H on the left to ^+2H on the right. This therefore gives us an aspect ratio, A of 4. However, subglacial lakes have pretty large aspect ratios of magnitudes greater than 10 [8] [4]. We decided to work with this aspect ratio of 4 because we wanted to make it computationally tractable and to limit confinement effects in the x-direction for the case when we have vertical convection that results from geothermal flux at the bottom of the lake. This value of aspect ratio 4 is the lower bound for large aspect ratios. T_f is the mean lake water temperature at the top boundary which is equivalent to the melting temperature of ice.

With the setup in figure 3, We expect a competition between vertical convection driven by the geothermal flux and horizontal convection driven by the horizontal temperature gradient along the tilted ice roof due to the pressure-dependence of the freezing temperature. We will use numerical simulations to try to understand when and which one of the two convections dominate and we should be able to
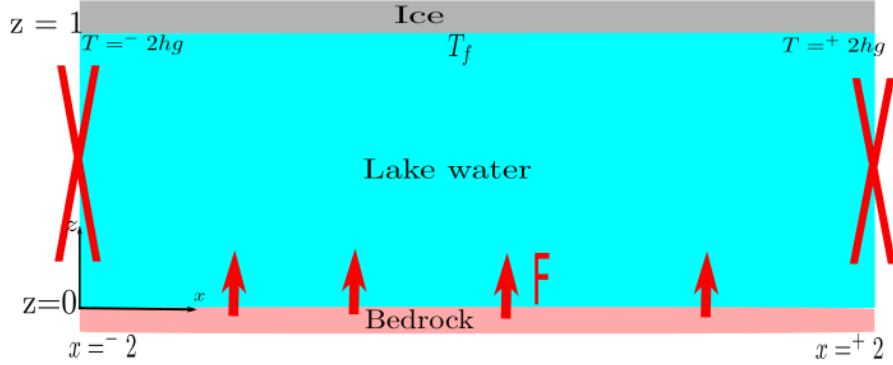
Figure 3: A simplified model with the all the applied boundary conditions for our study. F is the flux at the bottom of the lake arising from geothermal heating, big red crosses on the sides implies no flux on the side. The domain is of depth 1 (0 - 1) and length 4 ($^-2 - ^+2$). x,z coordinates and temperature difference at the top are in non-dimensional form. Non-dimensionlisation of variables is discussed in section 2.5

identify the transition point from one type of convection to the other.

2.2 Governing equations

We model two regimes of convection, that is, vertical and horizontal convection in a subglacial lake using the simplest forms of Navier stokes equations in Boussinesque approximation. These governing equations of fluid flow motion in dimensional form take the form below;

$$\frac{\partial \mathbf{u}}{\partial t} + \mathbf{u}.\nabla \mathbf{u} = -\frac{1}{\rho_0}\nabla p + \nu\nabla^2 \mathbf{u} - \frac{\rho}{\rho_0}g\hat{k} \tag{2.2}$$

$$\nabla.\mathbf{u} = 0 \tag{2.3}$$

$$\frac{\partial T}{\partial t} + \mathbf{u}.\nabla T = \kappa\nabla^2 T \tag{2.4}$$

Where ρ_0 is the reference density of the fluid in our case $\rho_0 = 1gcm^{-3} = 1000kgm^{-3}$, ρ is the density of fluid at given time and position in the volume of the fluid, $\mathbf{u}$ is the fluid velocity field vector in two dimensions ie $\mathbf{u} = u(x,z)$, T - temperature of fluid. ν and κ are respectively the kinematic viscosity and the thermal diffusivity, g is the acceleration due to gravity acting downwards opposite to normal vector $\hat{k}$. $\frac{\partial}{\partial t}$ denotes time derivative of velocity and temperature variables whereas ∇ is the gradient operator

Equations 2.2 and 2.3 are well known as the incompressible Boussinesq equations. Equation 2.2 describes the conservation of momentum in the flow where as the equation 2.3 is the incompressibility constraint on the flow, it is also referred to as the continuity equation. Since we are working with a 2-D domain, we neglect the effects due to the rotation of the earth, therefore the term due to Coriolis force in equation 2.2 is dropped. We assume that density variations in the fluid(subglacial water) are small in comparison with the velocity gradients such that from conservation of mass, we deduce equation 2.3. The equation 2.4 is the heat equation that describes propagation of heat in the fluid in terms of the spatial and temporal evolution of the temperature field. The left hand side of equation 2.4 describes the transport of heat in the fluid by advection whereas the right hand side of equation 2.4 describes the transport of heat by diffusion of temperature.

The equation of state is approximated by

$$\rho = \rho_0(1 - \alpha(T - T_0)) \tag{2.5}$$

where α is the thermal expansion coefficient T_0 is the reference temperature which is the average(mean) temperature at the top of the lake that is at $z = H$. T_0 is given by $T_0 = \frac{1}{L}\int_0^L T(z = H)dx$. This assumes that the density variations are very small and so can be approximated by a linear temperature dependency that takes the form of equation 2.5

2.3   Boundary and initial conditions

Equations 2.2, 2.3 and 2.4 can be solved by applying appropriate boundary conditions related to our problem. The following boundary conditions are used to define our problem.
We apply no slip boundary conditions,

$$\mathbf{u}(z = 0) = \mathbf{u}(z = H) = 0; \mathbf{u}(x = -2H) = \mathbf{u}(x = 2H) = 0 \tag{2.6}$$

No flux on the sides such that at $x = -2H, 2H$
$k\nabla T.\hat{x} = 0$, that is,

$$k\frac{\partial T}{\partial x} = 0 \tag{2.7}$$

We impose freezing temperature at the top of the lake such that the temperature T at the top ($z = H$) is equal to the fusion temperature(freezing temperature of water) i.e

$$T(z = H) = T_f(x) \tag{2.8}$$

Similarly, to be consistent with no flux boundary condition on the sides, we impose a sinusoidal temperature function at the top (z=H) such that the temperature on the top left is minimum and temperature on the top right is maximum. This temperature oscillates between $^-2 * hg$ and $^+2 * hg$

$$At \quad z = H : T = \frac{hg.A}{2}\sin(\frac{\pi x}{A}) \tag{2.9}$$

At the bottom, we impose a geothermal heat flux

$$-k\frac{\partial T}{\partial z} = F \tag{2.10}$$

where F is the flux which is the control parameter. Note that the gradient is negative because the flux imposes a temperature that is warmer at the bottom and decreases upwards.

For the initial conditions we shall take that the fluid is at rest and we impose also a sinusoidal initial temperature (in equation 2.12) which is kind of consistent with our boundary conditions of no flux on the sides and temperature gradient between the two opposite sides on the top.

$$u(t = 0) = 0 \tag{2.11}$$

$$T(t = 0) = \frac{hgA}{2}\sin(\frac{\pi x}{A}) + (1 - z) \tag{2.12}$$

where hg is the dimensionless horizontal temperature difference between the top left and right of the lake, A is the aspect ratio (L/H = 4). x and z the two dimensional coordinates.

2.4   The base static state

The base static state is when there is no velocity and assuming steady state, i.e., $\mathbf{u} = 0$ and $\frac{\partial}{\partial t} = 0$. It is a good idea to think about the base static state because it gives an idea of how the system would look like if there were no velocities. Equation 2.2 in the base static state yields

$$-\frac{1}{\rho_0}\nabla p = \frac{\rho}{\rho_0}g\hat{z} \text{ or } \frac{1}{\rho_0}\frac{\partial p}{\partial z} = \frac{\rho}{\rho_0}g\hat{z}$$

Giving;

$$\frac{\partial p}{\partial z} = -\rho g\hat{z} \tag{2.13}$$

Equation 2.13 is the hydrostatic equilibrium equation for the system. Equation 2.4 in base static state yields;

$$\kappa\nabla^2 T = 0 \tag{2.14}$$

where κ is the thermal diffusivity.

Equation 2.14 can as well be written as;

$$\kappa\left(\frac{\partial^2 T}{\partial x^2} + \frac{\partial^2 T}{\partial z^2}\right) = 0 \tag{2.15}$$

Equation 2.15 is the thermal diffusion equation. We seek the diffusive solution to this equation using our imposed boundary and initial conditions. We look for the solution of the form;

$$T(x,z) = \frac{hgA}{2}\sin(\frac{\pi x}{A})Z(z) + (1-z) \tag{2.16}$$

Recall that our domain is defined such that x ranges from ^-2H to ^+2H and z is from 0 to H (aspect ratio = 4). The task here is to find the unknown function Z(z). We substitute equation 2.16 into equation 2.15 and apply the boundary conditions discussed above. After some mathematical manipulations, we find the diffusion solution as shown in equation 2.17.

$$T(x,z) = \frac{hgA}{2\cos(\frac{\pi}{A})}\sin(\frac{\pi x}{A})\cos(\frac{\pi z}{A}) + (1-z) \tag{2.17}$$

Equation 2.17 is the solution to the diffusive state and can be used as an initial condition in our simulations. We find it interesting to have an initial condition with the diffusive solution rather than just an approximate solution however, we use the initial condition defined by equation 2.12 in our simulations because it is more stable for very high Rayleigh numbers and so the simulations do not blow up easily during the transient.

2.5 Non-dimensionalization of the governing equations

Nondimensionalization of equations 2.2, 2.3 and 2.4 is done by choosing characteristic scales for the length l, H, time t , velocity u , pressure p , and temperature T and perform a change of variables. This helps to give the resulting equations with non dimensional variables. Nondimensionalization of equations 2.2, 2.3 and 2.4 has an advantage that physical simulation times and tolerances tend to be easy to set when performing numerical simulations. Non-dimensionalising equations also has an advantage of reducing on the number of input variables in the Navier Stokes equations such that we deal with few input variables that are optimal to interpret.

2.5.1 Choosing characteristic scales

- **Characteristic Length Scale**
  We choose the characteristic length of H which is equal the depth of the fluid such that the non-dimensional length variable $\hat{x} = \frac{x}{H}$, and $\hat{z} = \frac{z}{H}$ giving $x = H\hat{x}$, and $z = H\hat{z}$

- **Characteristic time Scale**
  Characteristic time scale chosen here is the diffusive time scale $t = \tau_\kappa\hat{t}$ where $\tau_\kappa = \frac{H^2}{\kappa}$.

- **Characteristic velocity Scale**

  Characteristic velocity is simply defined as the ratio of characteristic length to characteristic time. We thus get a characteristic velocity of $u_\kappa = \frac{\kappa}{H}$ such that $u = \frac{\kappa}{H}\hat{u}$

- **Characteristic pressure Scale**

  We use dynamic pressure scale $p(x, z) = p_i(x) + \rho_0 g(H - z) + \Delta p \hat{p}$ where $p_i(x)$ is the ice overburden pressure given by $p_i(x) = p_{atm} + \rho_i g(H_i^* - x \tan\phi)$ and $\Delta p = \rho_0 u_\kappa^2$. P_{atm} is the atmospheric pressure exerted on the surface of ice, ρ_i is the density of ice, H_i^* is the thickness of ice and ϕ is the ice slope. Since we consider a rectangular geometry for simplicity, we assume $\phi = 0$ such that the term $x \tan\phi$ is equal to 0

- **Characteristic temperature Scale**

  The characteristic temperature scale T here is typically defined using the mean temperature difference in the fluid between lower(bottom) and upper(top) boundary $\Delta T = \frac{FH}{k}$. We define T as function of a dimensionless variable such that $T = \bar{T}_f + \Delta T \hat{T}$ where $\bar{T}_f$ is the mean freezing temperature at the top (interface between subglacial lake and ice) and T is the temperature in the bulk of the lake water.

2.5.2 Coordinate transformation (change of variables)

Coordinate transformation is performed as below using the above characteristic scales;

$$\nabla = \tfrac{1}{H}\hat{\nabla}, \ \nabla^2 = \tfrac{1}{H^2}\hat{\nabla}^2$$
$$\tfrac{\partial}{\partial t} = \tfrac{\kappa}{H^2}\tfrac{\partial}{\partial \hat{t}}$$
$$\tfrac{\partial u}{\partial t} + u.\nabla u = \tfrac{\kappa^2}{H^3}\left[\tfrac{\partial \hat{u}}{\partial \hat{t}} + \hat{u}.\hat{\nabla}\hat{u}\right] \text{ and}$$
$$\rho = \rho_0(1 - \alpha\Delta T\hat{T}) \text{ with } \Delta T = T - \bar{T}_f = \tfrac{FH}{k}$$

Substituting the transformed coordinates and characteristic scales into equations 2.2, 2.3 and 2.4 yields;

$$\frac{\kappa^2}{H^3}\left[\frac{\partial \hat{\mathbf{u}}}{\partial \hat{t}} + \hat{\mathbf{u}}.\hat{\nabla}\hat{\mathbf{u}}\right] = \frac{-1}{\rho_0 H}\hat{\nabla}\left[p_i + \rho_0 g(H - H\hat{z}) + \frac{\rho_0\kappa^2}{H^2}\hat{p}\right] + \frac{\nu\kappa}{H^3}\hat{\nabla}^2\hat{\mathbf{u}} - (1 - \alpha\Delta T\hat{T})g\hat{k} \quad (2.18)$$

$$\hat{\nabla}.\hat{\mathbf{u}} = 0 \quad (2.19)$$

$$\frac{\kappa}{H^2}\frac{\partial}{\partial \hat{t}}(\bar{T}_f + \Delta T\hat{T}) + \frac{\kappa}{H^2}\hat{\mathbf{u}}\hat{\nabla}(\bar{T}_f + \Delta T\hat{T}) = \frac{\kappa}{H^2}\hat{\nabla}^2(\bar{T}_f + \Delta T\hat{T}) \quad (2.20)$$

$\hat{k}$ is a unit vector pointing upwards opposite to the acceleration due to gravity g. Rearranging and introducing non-dimensional constants yields;

$$\frac{\partial \hat{\mathbf{u}}}{\partial \hat{t}} + \hat{\mathbf{u}}.\hat{\nabla}\hat{\mathbf{u}} = -\hat{\nabla}\hat{p} + P_r\hat{\nabla}^2\hat{\mathbf{u}} + R_a P_r \hat{T}\hat{k} \quad (2.21)$$

$$\hat{\nabla}.\hat{\mathbf{u}} = 0 \quad (2.22)$$

$$\frac{\partial \hat{T}}{\partial \hat{t}} + \hat{\mathbf{u}}.\hat{\nabla}\hat{T} = \hat{\nabla}^2\hat{T} \quad (2.23)$$

In equations 2.21 - 2.23 we have introduced the dimensionless constants, $P_r = \frac{\nu}{\kappa}$ and $R_a = \frac{\alpha g\Delta T H^3}{\kappa\nu}$ which are respectively the Prandtl and Rayleigh constants. Equations 2.21, 2.22 and 2.23 are the gorverning equations in dimensionless form and the control parameter in these equations are the Rayleigh number, Prandtl number and the aspect ratio ($A = \frac{H}{L}$). For horizontal convection resulting from the temperature difference at the top surface, we define a horizontal Rayleigh number as $R_{aL} = \frac{\alpha g\Delta T_L L^3}{\kappa\nu}$. It should be noted that in equation 2.21, we have taken the simplest case when there is no ice slope that is $\phi = 0$. But in reality $\phi \neq 0$. In subsequent studies, we recommend this slope to be taken into account.

2.6 Dimensionless boundary and initial conditions

We use the characteristic scales discussed in section 2.5 to define the boundary and initial conditions in dimensionless form.

- The no slip boundary condition in dimensionless for becomes;

$$at \quad z = 0, 1 \quad and \quad x =^- 2,^+ 2, \quad \hat{u} = 0 \tag{2.24}$$

- No flux on the sides boundary condition in dimensionless form takes the form below;

$$At \quad x = 0, L, \quad \frac{\partial \hat{T}}{\partial \hat{x}} = 0 \tag{2.25}$$

- The boundary condition due to imposed geothermal heat flux at the bottom of the lake takes the form;

$$at \quad z = 0 \quad \frac{\partial \hat{T}}{\partial \hat{z}} = \frac{-FH}{k} \cdot \frac{1}{\Delta T} \tag{2.26}$$

The flux F imposed at the bottom due geothermal heating induces a temperature difference $\Delta T = \frac{-FH}{k}$ between the top and bottom of the fluid. This causes a temperature diffusion from the bottom to the top surface. This redefines the boundary condition such that;

$$at \quad z = 0, \quad \frac{\partial \hat{T}}{\partial \hat{z}} = -1 \tag{2.27}$$

There fore the dimensionless flux value imposed at the bottom boundary of our domain is $F = 1.0$

- Dimensionless horizontal temperature gradient at the ice - water interface, hg is defined as;

$$hg = \frac{\delta T}{\Delta T} \tag{2.28}$$

where δT is the dimensional temperature gradient between the top left and top right of the domain, ΔT is the temperature difference between the top and the bottom of the domain induced by a flux, F at the bottom boundary.

3 Methodology

3.1 Numerical model: Nek5000

During this study, we perform all our simulations using a numerical code, Nek5000. Nek5000 is an open-source code that was developed by Fischer in 2008 [17]. It is written in Fortran77 and C languages. It uses MPI for passing messages (but can be compiled without MPI for serial applications) [17]. The computational approach used by Nek5000 is that of the spatial discretization that is based on the spectral element method(SEM) which has a high order weighted residual technique similar to the finite element method. This allows Nek5000 to offer a high level of accuracy with fewer grid points compared to Finite Element methods. Hence, the Spectral Element Method used by Nek5000 exhibits an advantage of computational efficiency for high-fidelity simulations [18]. In Nek5000, the global domain Ω is divided into a finite number of non-overlapping elements Ω^e on which the solution is approximated by a polynomial expansion following the Galerkin approach, and global continuity at the element boundaries is enforced [18]. The basis functions in Nek5000 are determined by the Lagrangian interpolation based on Legendre polynomials P_N of order N. Furthermore, the $P_N - P_{N-2}$ formulation proposed by Maday and Patera [19] is employed, where the basis functions associated

with the pressure field are two polynomial orders below N, which is the order used for the velocity field, effectively eliminating spurious pressure modes[18]. It should be noted that one of the greatest advantages of the SEM is the exponential decay of the error as the order of the polynomial increases[17]. Nek5000 basically solves the unsteady incompressible Navier stokes equations with forced or natural convection heat transfer, in both stationary or time dependent geometry [17]. The solution variables solved in Nek5000 are the fluid velocity,$\mathbf{u}=(u_x, u_z)$, pressure,p and temperature,T. Nek5000 can also be used for heat transfer problems. We use the results of the solved physical variables ($\mathbf{u}$,p,T) to characterise and describe our fluid system.

3.2 Number of cores test

To know which number of cores is optimal when running Nek simulations on a supercomputer, we performed a number of cores test to identify which cores we can use efficiently for our simulations. Several simulations were performed with same input parameters but varying number of cores. Table 1 show the results of the simulation time for each number of cores. The results are represented in

No. of cores	Simulation time[s]
1	2007.2
2	993.3
4	513.9
8	287.1
16	162.9
32	127.1

Table 1: Number of cores test with the simulations run using same input parameters of $Ra = 10^6$, $Pr = 1$, $hg = 0.25$, $F = 0$ and $finitime = 0.5$ but different number of cores.

figure 4. Figures 4a and 4b represent the results on a linear and log scale respectively.
The main conclusion from the number of cores test is that the scaling is quite good for example

(a)   (b)
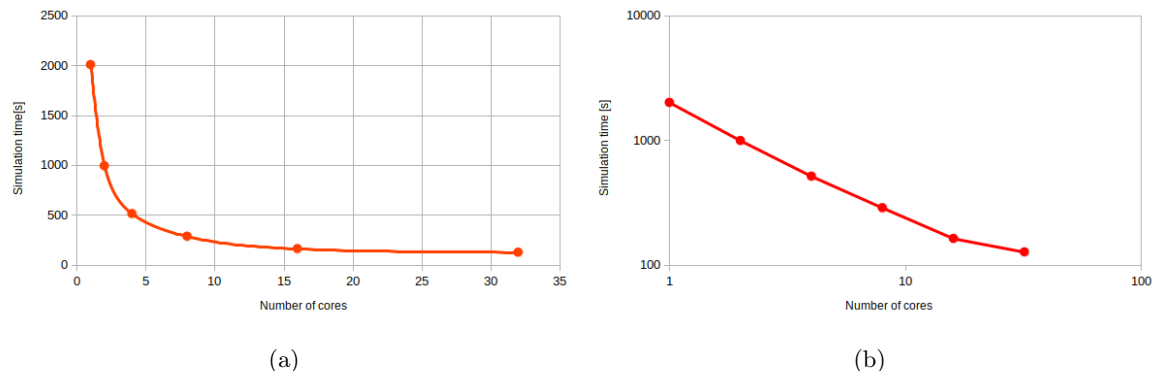
Figure 4: Number of cores test

going from 1 to 2 cores, the simulation time is almost divided by two which means that the simulation runs much faster. Also from 2 to 4 t0 6 to 8 to 16 cores, the time keeps on being reduced by a half. Moving from 16 to 32, the relative improvement is not like before, it is about 30% faster (not 50% as before). So for our spectral resolution (at the moment) of 1600 elements par node with 80 elements in x and 20 elements in z, shows that 16 cores is a good number to work with, so all our simulations are performed using the number of cores as 16.

3.3 Numerical simulations

We use the Direct Numerical Simulations(DNS) approach to perform all our numerical simulations whereby all flow scales are resolved on the numerical grid. We use a mesh grid of 1600 elements on each node with 80 elements in the x-axis and 20 elements in the z-axis. We have a large number of element close to the boundaries so as to increase element resolution close to these boundaries. The spectral resolution of the mesh is set to 8 although for very high values of Ra, the resolution can be modified to 10 (or even 12 to allow the simulation run). Subglacial lakes do have large aspect ratios of orders of magnitude greater than 10, we chose to work with an aspect ratio of 4 as a starting point and we as well performed some few simulations with aspect ratio 8 to compare the results of the two values. Simulations are performed with Rayleigh numbers of $10^5, 10^6, 10^7, 10^8$ and 10^9. We use a fixed input Prandtl number of 1 ($Pr = 1$) for all our simulations. Dimensionless horizontal temperature gradient values used are small values less than 1 as reported in [8]. So, for each Rayleigh number, we perform six simulations with different temperature gradient values of 0, 0.001, 0.01, 0.1, 0.5 and 1.0 such that we have in total 30 sets of simulations. We use the data generated by Nek5000 for each simulation and do a post analysis using python. After simulations are performed, data sets at each probe on the entire grid was saved in a big data file for post analysis using python. This data set included records of variables of temperature, velocity, kinetic energy, vorticity, enstrophy and convective flux. Global averaging was done using a routine built in Nek5000 whereas time and space averaging was done using Numpy, a python module during our postprocessing. The results are presented and discussed in the results and discussion section.

4 Results and discussion

In this section we present the results from our numerical simulations of the fluid dynamics of subglacial lakes. The results presented here are model results thus they are a prediction of what we would expect in subglacial lakes but are rather not factual results. With expeditions to Antartic subglacial lakes planned for the near future, results from insitu measurements could be used to validate our model results.

4.1 Average temperature evolution in the fluid domain

From the graphs in figure 5, we observe in general a temperature drop between the time of 0 - 0.4 and then the temperature remains constant. Initial drop in temperature is due to the initial temperature condition imposed in our simulations. It means that initially we imposed a temperature that is slightly higher than that of the entire fluid domain. From figure 5a, on average the temperature decreases with an increase in the horizontal temperature difference(hg) at the top boundary. The flux imposed at the bottom warms up the fluid but overall, the mean fluid temperature is slightly higher than the temperature of the coldest fluid(top left of our domain). This is because downwelling convection from the top left is very efficient, such that when the fluid from the top left descends, it decreases the overall temperature of the liquid below. That is why we see the temperature of the entire domain decreasing with time before it becomes steady implying that increasing hg increases the cooling effect. We refer to the region where the temperature is decreasing with time as the **transient state** and the region where the temperature is steady as the **dynamical statistical steady state**. Dynamic because there is fluid movements in the domain and also we can describe some features of the system by computing statistics of the flow implying statistical. Therefore it is a steady state in the sense of the statistics and that is why we referred it to as dynamical steady state. For hg values between 0 - 0.1, the values of temperature variation are very close to each other as we see the curves are not much separated. Note that in figure 5b for $Ra = 10^9$, the graph initially is different from the others because we used a different initial condition where by we started with zero temperature everywhere. That is why in this case the temperature of the fluid domain initially warms up (due to geothermal flux heating) and then after some time it stabilises at equilibrium state. We used a different initial condition because
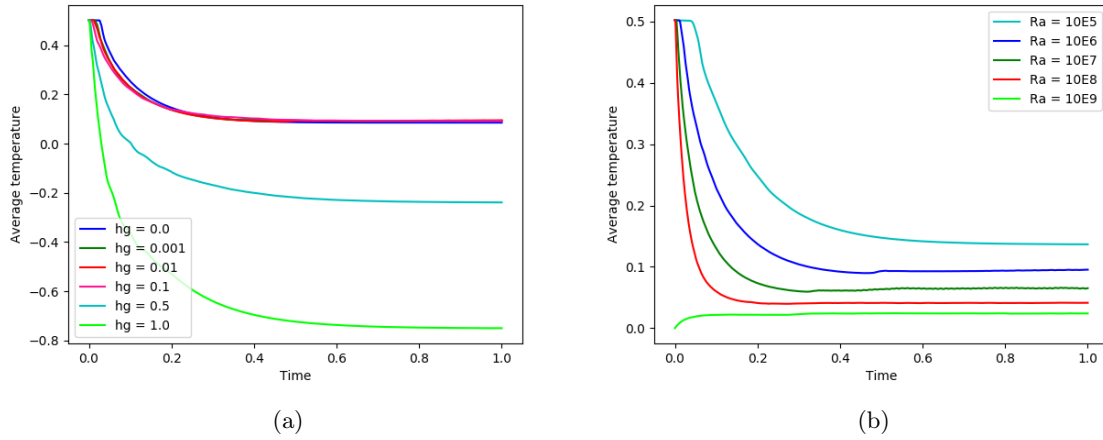
Figure 5: Volume average temperature evolution in the fluid domain as a function of time. Time scale used here is the diffusive time scale. (a) is the volume average temperature for simulations of $Ra = 10^6$ and different horizontal temperature gradient (hg) values. (b) Compares the temperature evolution for a given value of $hg = 0.01$ for different Rayleigh numbers. From figure 5b, we can see that increasing Ra makes the mean temperature tend to 0, which is the average temperature of the top boundary. This is a well known results from RBC when the bottom flux increases. The top boundary layer thins while maintaining the same flux, such that the temperature difference between the top boundary and the bulk decreases.

the first one was very turbulent and chaotic making the simulation crush easily. We therefore used an initial condition that is relatively stable initially for this high value of Ra. All further analysis of time averages is done using the steady state solution, i.e., time averages are computed starting from the time when we have achieved steady state. We use averages or statistics because they characterize the flow for all times for a given simulation. Since we are interested in understanding what takes place in the entire fluid domain at steady state, we compute the steady state time average temperature and plot it as a colormesh for x and z directions. The color scales increases with increasing hg value. The results are shown in figure 6 and 7. The figure 6 compares the steady state temperature at different hg values whereas figure 7 compares steady state temperature for different Rayleigh numbers.

Generally we see that moving from $hg = 0$ to $hg = 1.0$, we move from a convection that is typically Rayleigh-Bernard convection driven by a geothermal flux at the bottom to a horizontal convection driven by a large temperature gradient between the top right and top left of our defined fluid domain. At low hg values (0 - 0.01) in figure 6, the Rayleigh-Bernard convection is seen to dominate and we are able see plumes of warm fluid rising. The influence of the bottom geothermal flux heating can easily be seen. At hg=0.001 in figure 6, we see a plume rising on the left boundary where we expect cold water masses to be sinking, this is because the plume is inertia driven by the sinking plume in the middle that makes it (rising plume) to go up strongly compared to the sinking fluid from the top left. The inertia force thus overcomes the down falling cold water masses enabling the plume to rise where it would be expected to sink. Increasing hg values to 1, we move into a domain characterised by horizontal convection and we can see a uniform temperature domain with a temperature gradient between the top right and top left seen to play part. In this regime horizontal convection dominates and the influence of the bottom geothermal flux can be seen to be minimal though it still exists and still drives the fluid upwards implying that in reality we have both vertical and horizontal convection taking place. In figure 7, we observe that when we increase Ra, the color scale decreases with increasing Ra value. This is because when the bottom flux increases, the top boundary layer thins while maintaining the same flux, such that the temperature difference between the top boundary and the bulk decreases.
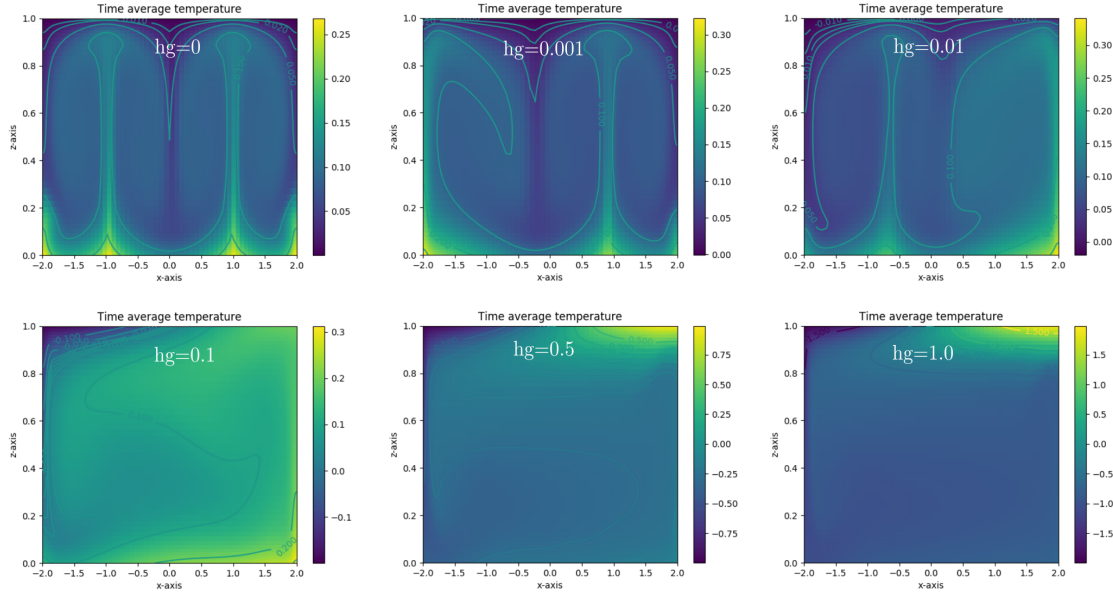
Figure 6: Steady state time average temperature distribution in the fluid domain plotted as a col-ormesh for $Ra = 10^6$ and different hg values. The color scale represents the temperature values and the contours are isothermal lines of constant temperature.

4.2 Volume average kinetic energy

The volume average kinetic energy was computed so as to give us an insight on the motion/dynamics and turbulence of the fluid. Kinetic energy is computed using mean square speeds (magnitude of velocities) given by the formula $K.e = \frac{1}{2}(u^2 + w^2)$, u and w being respectively the horizontal and vertical velocities of fluid motion. The results are presented in figure 8. From the two graphs we can observe that initially the kinetic energy of the fluid is zero consistent with our initial condition of zero speed everywhere in the fluid. The kinetic energy then increases rapidly with time, reaches a maximum value and then slightly drops to a lower value before remaining constant for the remaining time.The peak in the kinetic energy for different curves is what is referred to as the transient. This transient is important in numerical simulations because the fluid is going from non turbulent to a very turbulent state, it is during this stage that most simulations fail so it is important to choose better parameters to overcome this challenge especially for very high Rayleigh numbers and horizontal temperature gradients. The region where kinetic energy appears steady is the one we call the statistical steady state. Note that the kinetic energy at steady state is not zero implying that the fluid is still moving but less violently compared to the transient state. Overall the kinetic energy is seen to increase with Ra. This is because increasing Ra, increases the general turbulence of the fluid and the fluid masses move faster, thus increasing kinetic energy. From figure 8a, it is not very clear that kinetic energy increases with hg. In fact increasing hg from 0 to 1 implies a re-organisation of the flow that doesn't necessarily results in increased kinetic energy. However, as hg is further increased, kinetic energy increases because the dominant horizontal circulation intensifies.

4.3 Mean fluid flow

The mean flow of the fluid at steady state is computed using the root mean square of the speeds, 1.e., the time average velocity fields at steady state and we plot results using a color mesh as shown in figures 9 and 11. This is done to aid us see the evolution of our system as we change hg and(or)
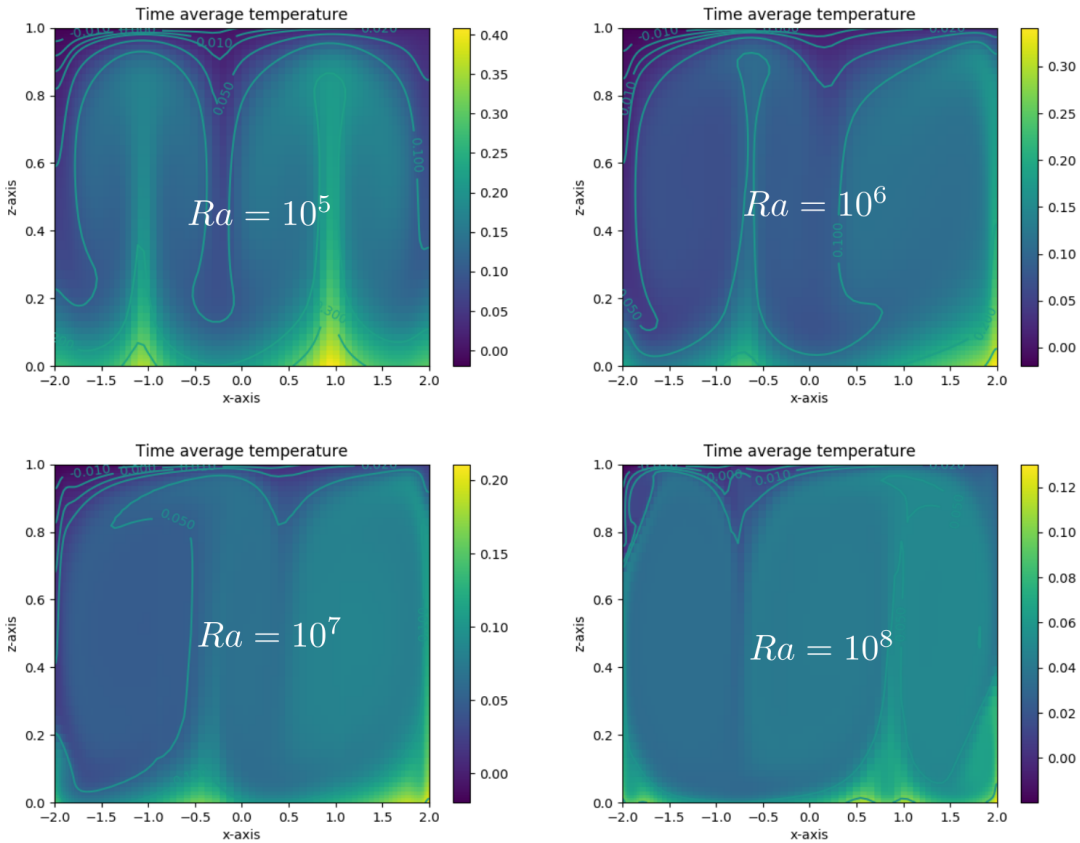
Figure 7: Steady state time average temperature distribution in the fluid domain plotted as a colormesh for $hg = 0.01$ and different Ra values. Once again The color scale represents the temperature values and the contours are isothermal lines of constant temperature.

Ra. The size and direction of the arrows superposed on mean flow show the magnitude and direction of the velocity. From figure 9, we can observe that as we increase from hg=0 to hg=1.0, in general we move from many convection cells (4 for hg=0) to a single uniformly distributed cell(hg=1). For hg value 0.01 and below, we have mostly Rayleigh Bernard convection and the cells are easily visible with fluid rising and falling. From hg=0.1, horizontal convection takes center stage and we can see the fluid moving counter-clockwise horizontally in the entire domain as one cell. On the sides we have warm water rising on the right side (where the temperature at the top is warm) and cold water masses falling on the left side (where the temperature is coolest).

A very interesting observation made is that as we move from hg=0 to hg=0.001, the biggest cell on left is moving in the clockwise direction yet we would expect it to mover in the anticlockwise direction. We observe as well water masses rising at the top left where the fluid temperature is coolest and at this point we would expect the cold water to be falling. Similarly to that we observe water falling from the top right corner (where temperature is warmest implying the liquid there is warmer and less dense so we would expect it to rise further or move leftwards). We tried to find an explanation to this unique behaviour and one of the explanations was it could be because the cell is inertia driven by the center cell and thus driving the cell to move in the counter opposite direction as observed. This inertia driving force outweighs the gravity force of falling water and this in general drives the fluid to move upwards at the top left and to balance the state, some water masses must fall on the right hand side of the domain. We also thought that this unique behavior could be due to existence of reversals
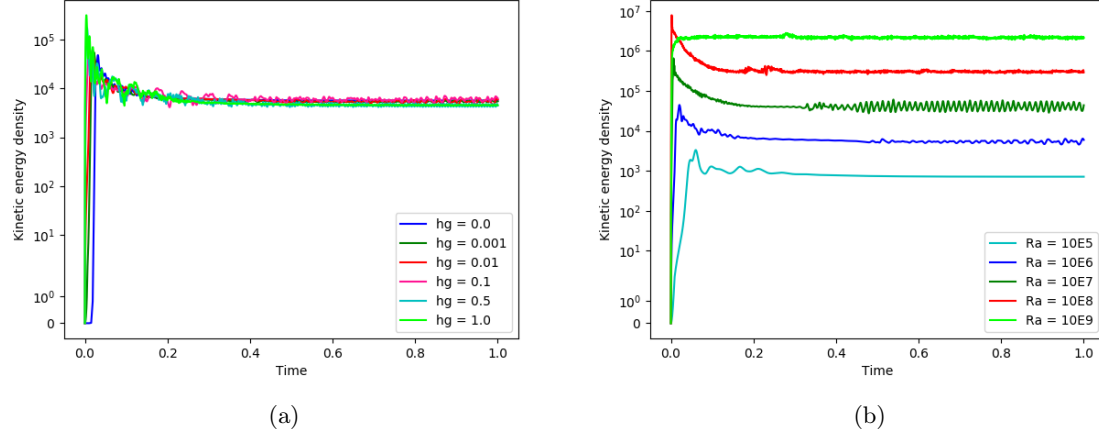
Figure 8: Volume average kinetic energy distribution in the fluid domain as a function of time. (a) Compares kinetic energy with different hg values for a fixed $Ra = 10^6$ while (b) compares kinetic energy for hg=0.01 for different Ra values. We choose to compare different Ra values at hg=0.01 in because hg=0.01 is quite relevant to subglacial lakes.
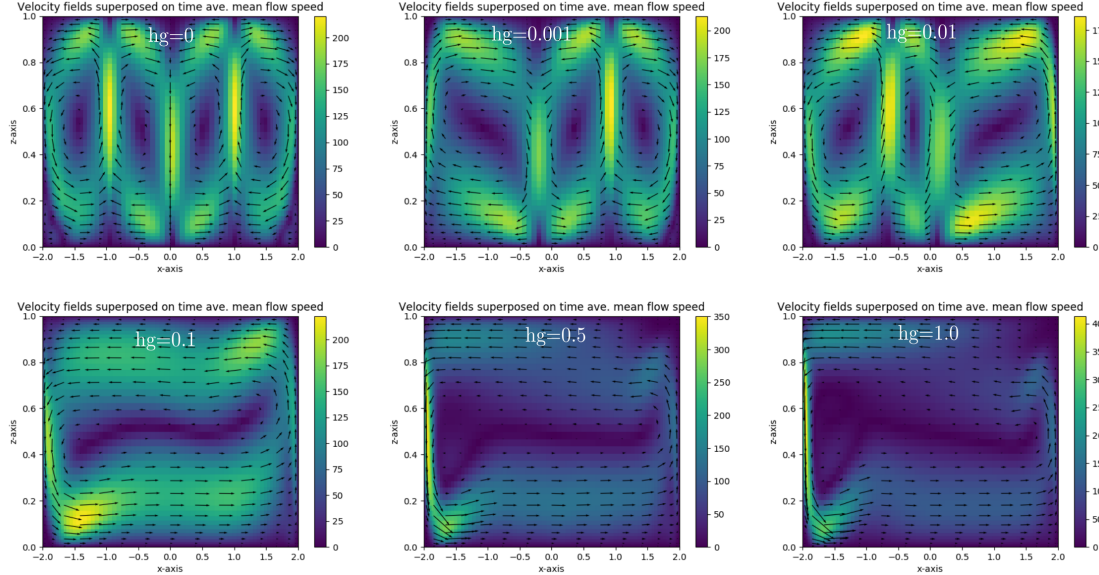
Figure 9: Time average mean flow plotted as a color mesh with vector fields superposed for $Ra = 10^6$, for different hg values

at steady state and we thought maybe there exist several solutions at steady state where the fluid flow keeps reversing. However, we checked for reversals using different approaches and the results indicated that there was no reversals at steady state. This allowed us to conclude that the clockwise movement of the large cell on the left at hg = 0.001 is inertia driven. To check for reversals, we re-did the time averaging such that we separated the time average values into three sub parts from the time when we start to have steady state (ISS) to the end other than have just one full time average as before. The three time averages we did were from (ISS to ISS+200), (ISS+200 to ISS+1000) and (from ISS+1000
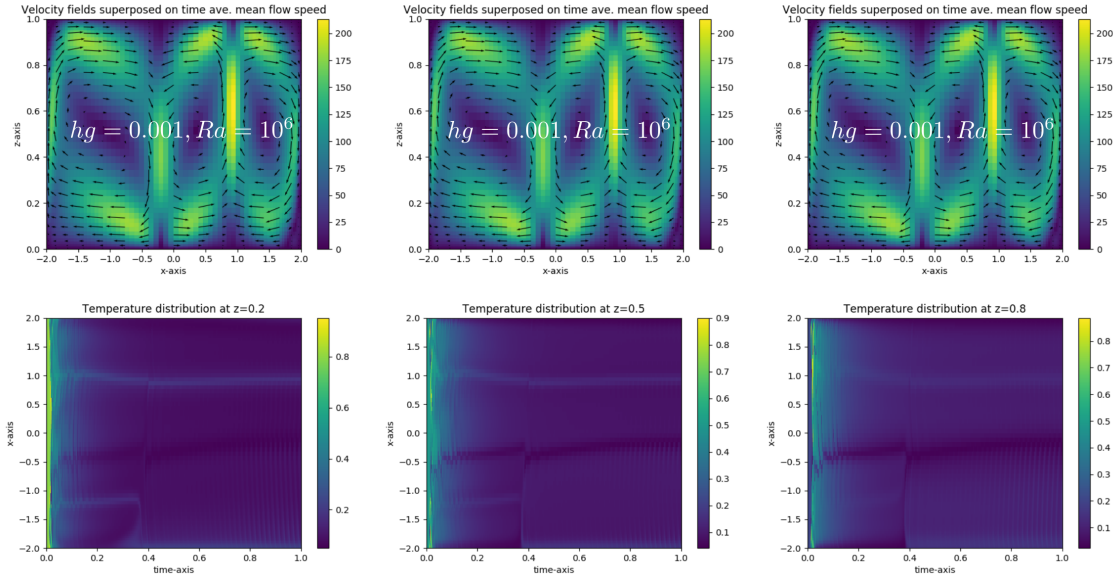
Figure 10: Reversals check: Top row show reversal check using different time averages at steady state and the bottom row show reversal check by looking at the time history of the temperature at given z position (of z=0.2, z=0.5 and z=0.8).

to ISS+3000). The results are shown in figure 10 (top row). The results show no change in the pattern of flow and thus we were unable to detect reversals using this approach. Another way to check for reversals, we chose 3 lines along z-axis, that is, at z=0.2, z=0.5 and z=0.8 and we looked at the time history of the temperature at these locations at steady steady. The goal of doing this was to be able to see whether warm and cold water patches were changing positions or not. If they were to change positions, then we would conclude that there are reversals in fluid flow else there exists no reversals. By looking at temperature as a function of x-axis and time and plotting the results as a colormesh in python, we obtained results in figure 10 (bottom row). Again we were unable to observe reversals and this drove us to conclude that there existed no reversals of mean flow at steady state and the unique flow of the large convection cell we see at hg=0.001 is basically due to inertia driving force from the center cell.

For the same Ra and hg value, re-running the simulation with a different initial condition of zero temperature and noise every where, we get a different solution and the direction of mean flow changes (figure 17 in appendix). This is because the system is non linear and thus changing the initial condition changes the mean flow of the the entire system.

Figure 11 shows the mean flow with velocity vectors superposed for hg=0.01 and comparing for different Rayleigh numbers. General observation we make from the figure is that the number of cells decrease from four (for $Ra = 10^5$) to three (for $Ra = 10^8$). The color scale increases with increasing Ra because increasing Ra increases the flow speed and thus the fluid flows faster. It is also important to note that as Ra increases, it increases the intensity of both vertical convection and horizontal convection. This is because horizontal Rayleigh number is related to Ra by $Ra_H = Ra * hg * A^3$ with A the aspect ratio. Clockwise motion of two cells at the extreme ends is observed for $Ra = 10^8$, there is a strong temperature gradient at the top and at the center and this leads to an anticlockwise circulation in the center cell and the other on the sides are clockwise where the temperature gradient is weakest. Just like before the explanation for this circulation is also centred around the fact the the cells are inertially driven by the centre cell and also by the flux at the bottom. At $Ra = 10^8$, we can
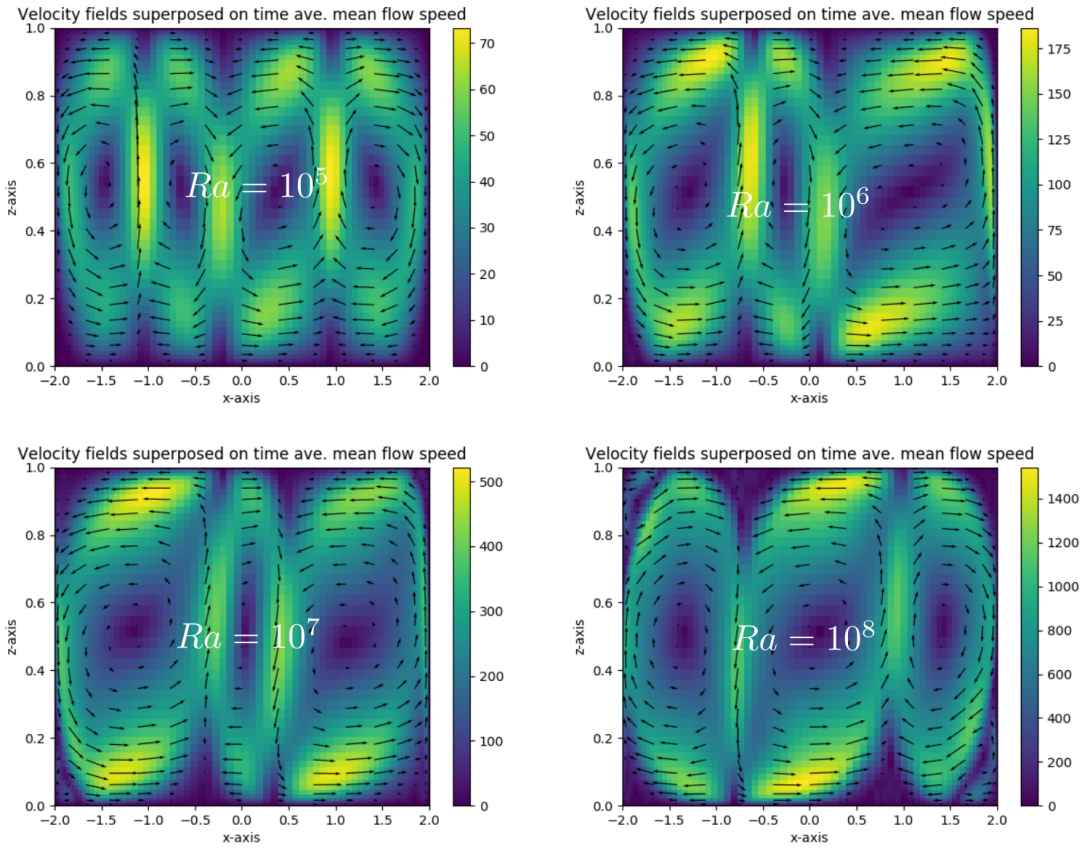
Figure 11: Time average mean flow plotted as a color mesh with vector fields superposed for fixed $hg = 0.01$ for different Ra values.

see small re-circulation cells at the top left and bottom right. To investigate the effect of aspect ratio on these results, we performed some simulations with $Ra = 10^6$ and hg=0, hg=0.001 and hg=0.01 to compare the results of two aspect ratios 4 and 8 (details in appendix).

4.4 Selected computed parameters

We were able to successfully run simulations with Nek5000 and obtained some interesting results as discussed in section results, but we are also interested in knowing how well we can characterise our fluid domain. Therefore we thought of some important variables that could aid us better understand the dynamics and behaviour of water in the subglacial lakes. Some of these variables included among others the Reynold's number because we were interested in understanding the overall turbulence intensity in the lakes, The Nusselt number which is to aid us understand transport of heat by convection in the entire fluid domain. Flux at the top boundary was as well computed as we expected this to give us some information on the freezing and melting at the ice-water interface of subglacial lakes. Finally we computed the mean equilibrium temperature of the fluid to give us some information on the thermal properties of the domain at steady state. These variables are discussed in details in the next subsections.
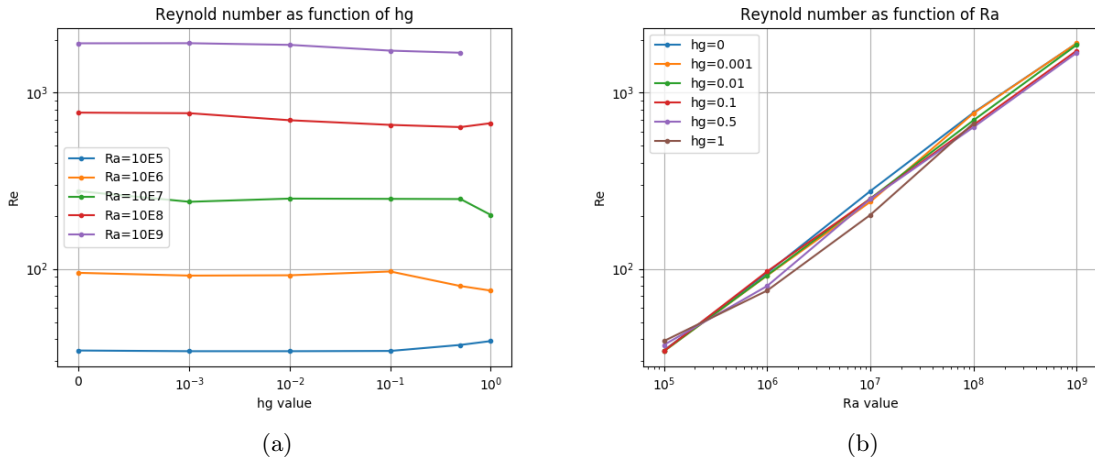
Figure 12: Dimensionless Reynold's number(Re) as a function of horizontal temperature gradient(hg) and Rayleigh number(Ra). For $Ra = 10^9$, one data point at hg=1.0 is missing due to lack of data that was caused by a failed simulation.

4.4.1 Reynold's number

Reynold's number is a dimensionless variable that compares inertial forces to viscous forces and it is used to characterize the extent of fluid flow properties[20]. Reynold's number is important in fluid dynamics because it provides information on the overall average turbulence intensity in a fluid domain, thus it helps to categorize laminar flows from the turbulent ones. We compute the Reynold's number using the root mean square velocities from the kinetic energy(K.E) expression as $Re = \sqrt{2K.E}$ where $K.E = \frac{1}{2}(u^2 + w^2)$: u and w being the horizontal and vertical velocities respectively. The computed Re is compared with hg and Ra and results are shown in figure 12. From figure 12a, it is observed that Re number is a weak function of hg, that is, for a given Ra value, Re does not vary much with hg and we can observe that the lines are almost horizontal (constant). In reality increasing hg, we expect Re to increase since hg is control parameter in horizontal Rayleigh number(Ra_H) implying that overall turbulence should increase as hg increases. However, since we are looking at subglacial lakes, where hg values are much smaller (0 - 1.0), it implies that for these very small hg values ($hg \leq 1$), changing from one hg value to another may only change the organisation of the system but does not change the overall intensity of turbulence in the fluid thus Re not varying much. But for very high hg values (applicable for fundamental fluid mechanics but not subglacial lakes), Re should increase as hg increases. We were able to perform two more simulations with hg=10 and hg=100 and we were able to observe that, truely the value of Re increased with hg. This result is shown in figure 19a in appendix. The explanation for this increase is that when hg is large enough (beyond subglacial lakes values), we start to inject in lots of energy into the system and the Re starts to increase with hg. Figure 12b shows variation of Re with Ra in loglog scale and we can clearly observe that Re is a strong function of Ra. In loglog scale we can see that the curves are almost linear which implies that there exist a power law between Re and Ra. We were able to compute the scaling law as shown in figure 19b in appendix for hg=0.01 curve. The power law expression is shown on the graph in figure 19b in appendix and we obtain the scaling between Re and Ra as $Re \sim 0.2 Ra^{\frac{11}{25}}$. This scaling is close to the one obtained in Rayleigh Bernard convection (RBC) studies, for which Re scales to Ra as $Re \sim Ra^{\frac{1}{2}}$ [21]. Our scaling for Re is close to RBC studies because for hg values less or equal to 1, the dynamics of the whole system is close to RBC than horizontal convection.

4.4.2 Equilibrium temperature
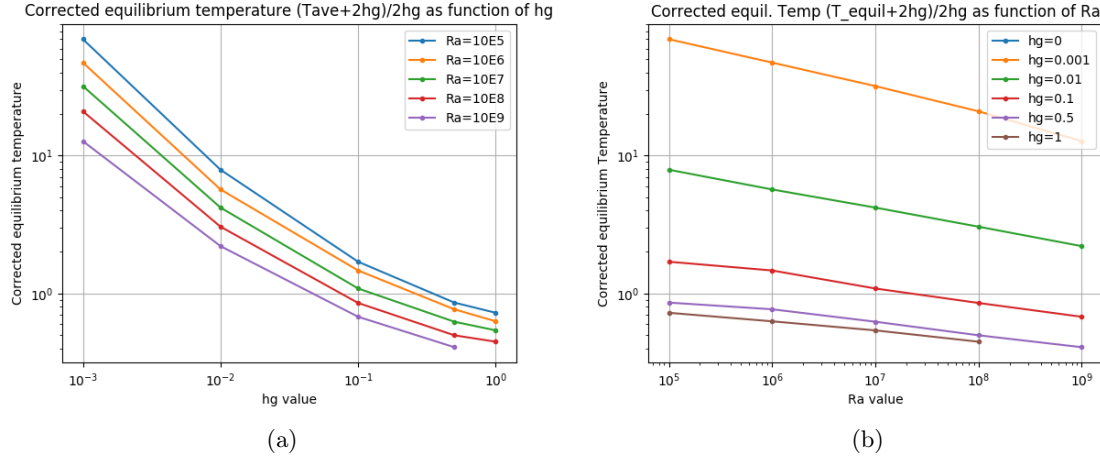
Figure 13: Equilibrium temperature in the fluid domain corrected above the minimum temperature in the domain (^-2hg) in dimensionless form as a function of horizontal temperature gradient(hg) and Rayleigh number (Ra).

The equilibrium temperature of our fluid domain was computed by taking the time average and volume average of the overall fluid temperature at steady state. The raw data obtained from this computation are plotted versus hg and Ra as shown in figure 20a in appendix. The equilibrium temperature initially varies very slowly with hg for different Ra values and then (from hg=0.1) decreases as hg increases. With Ra, generally the equilibrium temperature can be observed to decrease as Ra increases. Corrections were done to the raw data in order to guide how to establish a scaling between the equilibrium temperature and Ra. We did the correction on the equilibrium temperature by taking the raw values of equilibrium temperature and subtracting the minimum temperature in the entire domain that is ($T_{equil} + 2hg$). This is because we are interested in having temperature values that are either always positive or always negative. Also we normalize this corrected temperature by diving it by $2hg$ such that we define our equilibrium temperature (corrected and normalised) as $T_e = \frac{T_{equil} + 2hg}{2hg}$. The results in normalized non dimensional form are compared with hg and are shown in figure 13a. Figure 13b is comparing dimensionless equilibrium temperature with Ra. From figure 13a, We observe that for a given Ra, increasing hg decreases the overall equilibrium temperature of the fluid. This is because increasing hg implies we are increasing the temperature difference between the top left and top right. The top left liquid will become more cold and will sink reducing the overall temperature of the fluid in the domain whereas the less buoyant warm fluid on the top right will tend to stay up. We also observe that for a given value of hg, increasing Ra decreases the equilibrium temperature. This observations was also made in section 4.1. Same explanations to this observation applies as already discussed in section 4.1. A power fit law is computed (to obtain a scaling law between equilibrium temperature(T_e) and Ra) as shown in figure 20b in annexes. The power fit expression between T_e and Ra for hg=0.01 curve is also shown on the graph in figure 20b. This gives us a scaling law of $T_e \sim 38.5 Ra^{-\frac{7}{50}}$.

4.4.3 Temperature gradient on the top boundary

The temperature gradient(also called flux) at the top boundary is computed to give us an insight of what takes place at the ice-water interface. We expect this computed flux to give us some information on the freezing and melting at the top boundary. On average the flux at the top should be everywhere
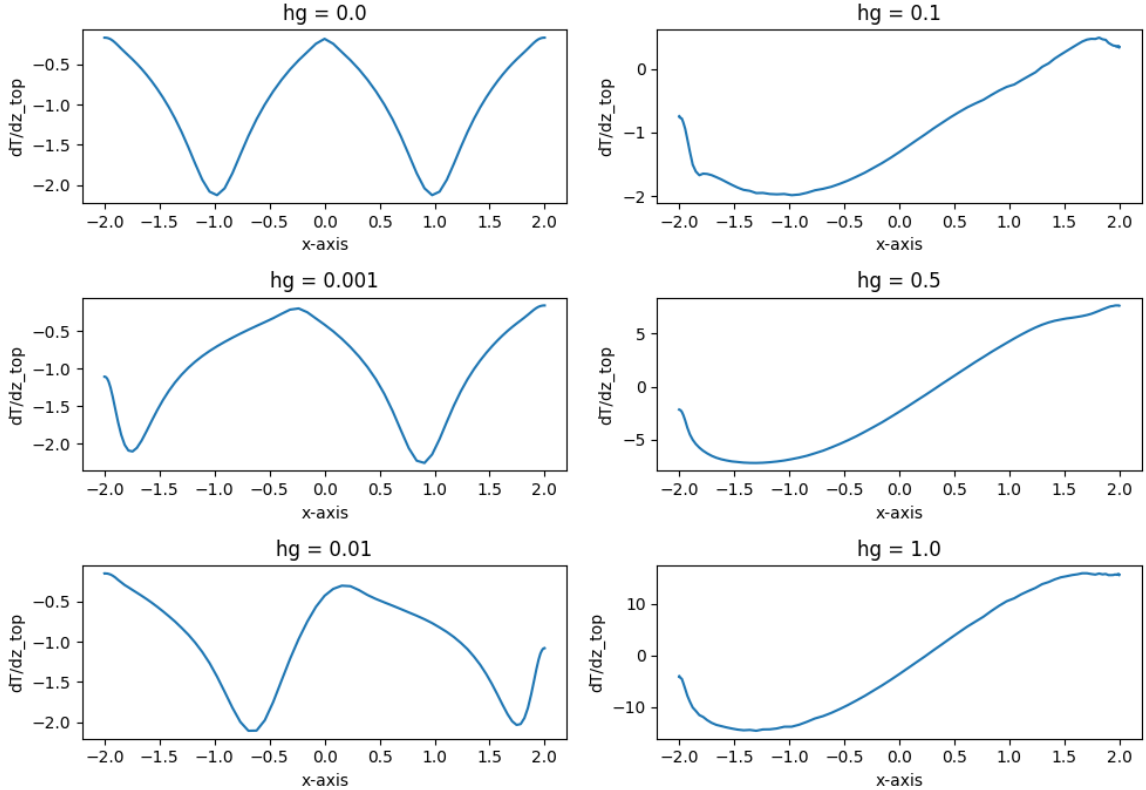
Figure 14: Time average temperature gradient on the top boundary at $Ra = 10^6$ and different values of hg. Temperature gradient is more negative on the left and positive on the right (for hg values from 0.1-1.0). When the temperature gradient is negative, the flux is positive implying that the flux is going out of the system. Therefore the flux is going out of the system from the top left and flux is coming into the system from top right. Flux going out of our domain from the top left thus does some work on melting the ice consequently, we have melting at the top left. At the top right, flux is coming into the system and thus we have freezing on this side.

equal to 1 because this is the flux we imposed at the bottom implying that at steady state, the rate of heat input from the bottom is equivalent to the rate of heat escape at the top boundary (bearing in mind that we imposed no flux on the side boundaries so no heat energy is supposed to enter or leave our system from the sides). To better characterise the top boundary using the flux, we compute the absolute temperature gradient at the top using the average of the absolute value using the equation 4.1

$$\frac{dT}{dz}_{top} = mean|\frac{dT}{dz}| \tag{4.1}$$

This computed value of absolute temperature gradient is then compared with hg and Ra and results can be seen on figure 15a and figure 15b. For hg values less or equal to 0.01, the temperature gradient at the top is close to 1 and constant with Ra implying we have steady state where the heat flux along the top boundary is always escaping the domain (i.e. the temperature gradient is negative everywhere while the heat flux is positive). For hg=0.01 and more, the temperature gradient increases with increase in hg and Ra. Figure 14 shows the variation of the temperature gradient/flux on the top boundary along the x axis. When we get a large value of absolute flux as it is the case for $hg > 0.01$, temperature gradient graphs (figure 14) reveals that we have strong melting on the left hand side where the flux is large and positive (Temperature gradient is more negative) and we have freezing on
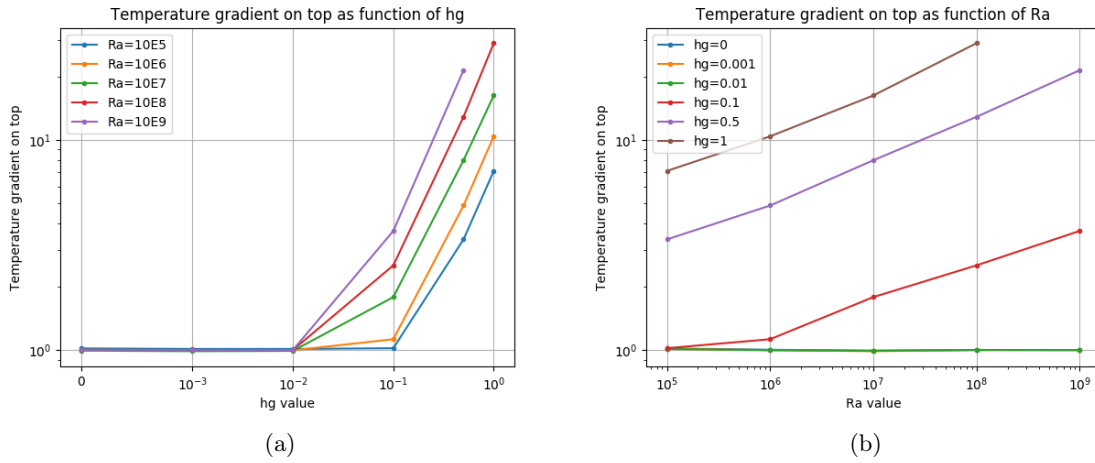
Figure 15: Variation of absolute temperature gradient (flux) on the top boundary as a function of hg and Ra.

the top right where the the temperature gradient is more positive(negative flux). From figure 15b, at high hg values, we can observe that there is a linear scale between flux and Ra. We computed this scaling using power-law fit and we found out that the temperature gradient at the top boundary scales with Ra by the relation; $\frac{dT}{dz}|_{top} \sim 0.3Ra^{\frac{1}{5}}$ (details on graph in figure 21 in annex). The main conclusion we make on this result of temperature gradient at the top boundary is that there is melting on the top left of our domain and there is freezing on the top right of our domain as seen in figure 14). This result is consistent with that in the literature for example [22] where the authors modelled flow and accreted ice in subglacial Lake Concordia, Antarctica and found out that melting in this subglacial lake occurred in most regions of the lake and where ice was thickest (in our case, this is the top left of our domain) and freezing occurred where overlying ice was thinnest (which is the top left in our case).

4.4.4   Nusselt number

To better improve our understanding of heat transport by convection in the our fluid domain, we computed the Nusselt number and compared it with both hg and Ra values. We also computed a scaling law relating the Nusselt number to Rayleigh number Ra. Different approaches(expressions) are used to compute the Nusselt number depending on the setup of the problem researchers are solving. We cite some few setups and their computation of Nusselt number which gave as a hint on how to come up with our own computation of Nusselt number that best suits our numerical problem. Gayen et al, 2014 [23] studied a problem on horizontal convection in which their setup was a rectangular domain with hot temperature imposed on the bottom left half and cold temperature imposed on the bottom right half with all the boundaries of the domain insulating. This setup studies horizontal convection just like ours though the difference here is that in our case we are imposing a flux at the bottom and a temperature gradient at the top boundary. They define their Nusselt number as the ratio of vertical heat flux to horizontal heat flux. Other studies [16], [13] and [20] define the Nusselt number depending on the set up of their problem. This aided as to come up with an expression to compute Nusselt number by defining it so as to fit our problem setup. We compute Nu using the flux on the cooling side (top left of our domain) using the expression in equation 4.2

$$Nu = \frac{-[\frac{dT}{dz} < 0]_{mean}}{hg} \tag{4.2}$$
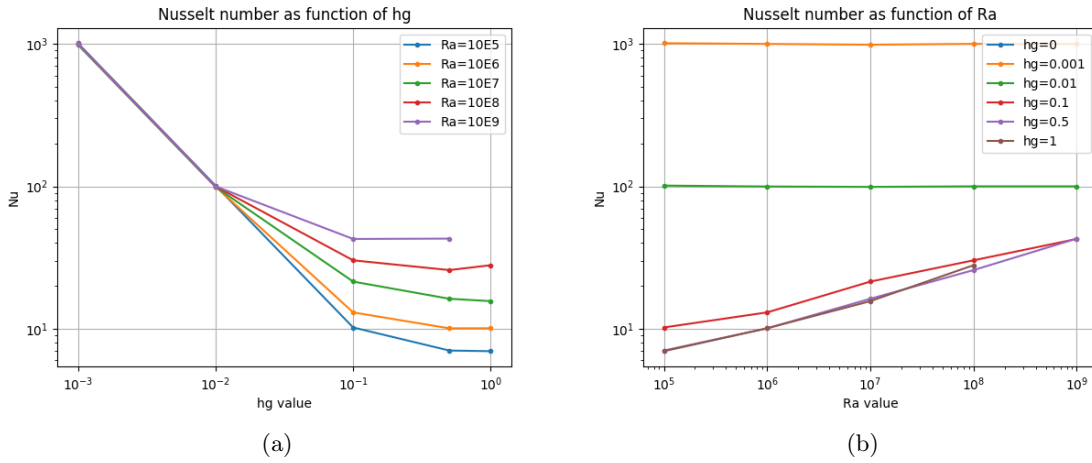
Figure 16: Dimensionless Nusselt number(Nu) as a function of horizontal temperature gradient(hg) and Rayleigh number(Ra).

where $[\frac{dT}{dz} < 0]_{mean}$ is the average flux on the cooling side of the our domain and hg is the horizontal temperature gradient at the top boundary. This Nu basically compares the vertical heat flux to the imposed horizontal heat flux due to hg. Using this expression, we compute Nu and compare it with hg and Ra. The results are shown in figure 16. For smaller hg, the vertical flux is not affected by the horizontal heat flux, if we increase the horizontal heat flux(by increasing hg), then Nu goes down. It then starts to become constant and it increases in very turbulent regimes where hg is high enough for example 10 or 100 (fundamental fluid mechanics problems). A scaling law between Nu and Ra is computed and we get a scaling of Nu $\sim 0.5 Ra^{\frac{1}{6}}$ (details on figure 22 in appendix). This scaling compares with that of Mullarney 2004 [15] where they studied horizontal convection in a rectangular domain in which a flux per unit area was applied on left half bottom of the domain and a uniform cooling temperature applied on the left bottom half of their domain with all other boundaries taken to be perfectly insulating. This study defines Nusselt number as the heat flux relative to that due to conduction along the length of the domain given by $Nu = \frac{\Delta T}{\delta T}$ and finds a scaling of Nu $\sim Ra^{\frac{1}{6}}$. Other studies like Yang [20], Gayen [23], with different horizontal convection studies setup find a scaling law of $Nu \sim Ra^{\frac{1}{5}}$

5   Conclusion

The dynamics of subglacial lake water is investigated using Numerical simulations with Nek5000 for $0 \leq hg \leq 1$ and $10^5 \leq Ra \leq 10^9$. The control parameters for these dynamics are; (i) The heating from the bottom of the lake due to geothermal flux. This influences the vertical Rayleigh Bernard convection quantified by the vertical Rayleigh number, Ra. (ii) The horizontal temperature gradient(hg) at the tilted ice-water ceiling that is caused by the difference in the ice over burden pressures between the top left and top right. The horizontal temperature gradient induces the horizontal flow (also known as horizontal convection) of the fluid in the domain. The fluid motion oscillates between vertical convection and horizontal convection depending on the horizontal temperature gradient. When the horizontal temperature gradient is small (less than 0.01), then vertical convection due geothermal flux heating dominates and we have basically Rayleigh Bernard convection taking place in the subglacial lake. When horizontal temperature gradient is large enough (greater that 0.01), then we have horizontal convection dominating and we have strong horizontal flow of the lake water. It has been shown from the results that increasing Ra and hg decreases the equilibrium temperature of the entire

fluid domain and the bottom temperature as well decreases. Further more it has also been shown that the overall intensity of fluid flow increases with increasing Ra though it is a weak function of hg for lower values of hg. For very high values of hg, the intensity of fluid flow increases with hg. Numerical simulations results reveal a strong negative temperature gradient (strong positive flux) on the side where the ice is thickest and a strong positive temperature gradient (strong negative flux) on the side where the ice block is thinnest. Thus we have strong melting on the side with positive flux and freezing on the side with negative flux that is to say we have melting at the top left of our defined domain and freezing at the top right of the domain. The results allowed us to compute the scaling between Re, equilibrium temperature, top boundary flux and Nu with the Rayleigh number, Ra. These variables were found to scale with Ra as; $Re \sim 0.2 Ra^{\frac{3}{11}}$, $T_e \sim 38.5 Ra^{-\frac{7}{50}}$, $\frac{dT}{dz}|_{top} \sim 0.3 Ra^{\frac{1}{5}}$ and $\sim 0.5 Ra^{\frac{1}{6}}$ respectively.

References

[1] Martin J. Siegert et al. Physical, chemical and biologicalprocesses in lake vostok and other antarctic subglacial lakes. *Nature*, 414:603–609, December 2001.

[2] Martin J. Siegert. Antarctic subglacial lakes. *Earth-Science Reviews*, 50:29–50, 2000.

[3] S.J. Livingstone J.S. Bowling and W.Chu J.Sole. Distribution and dynamics of greenland subglacial lakes. *Nature Commun*, 10:1–11, June 2019.

[4] L. A Couston. Turbulent convection in subglacial lakes. *Journal of fluid mechanics*, 915:A31, January 2021.

[5] M.R.Gorman M.J.Siegert, J.A.Dowdeswell and N.F.Mccintyrp. An inventory of antarctic subglacial lakes. *Antarctic Science*, 8:281–286, April 1996.

[6] G.K.A Oswald and G. Robin. Lakes beneath the antarctic ice sheet. *Nature*, 245:251–254, October 1973.

[7] I.R.Joughin B.E.Smith, H.A.Fricker and S. Tulaczyk. An inventory of active subglacial lakes in antarctica detected by icesat (2003–2008). *Journal of Glaciology*, 55(192):573–595, 2009.

[8] L. A Couston. M. Siegert. Dynamic flows create potentially habitable conditions in antarctic subglacial lakes. *Science advances*, 7 : eabc3972, February 2021.

[9] M. Balme P. Doran C.P. McKay K. Miljkovic D. Pearce M. J. Siegert M. Tranter M. Voytek C.S. Cockell, E. Bagshaw and J. Wadham. Subglacial environments and the search for life beyond the earth. *Antarctic Subglacial Aquatic Environments*, 192:129–148, 2011.

[10] Martin J. Siegert. Lakes beneath the ice sheet: the occurence, analysis, and future exploration of lake vostok and other antarctic subglacial lakes. *Annu. Rev. Earth Planet. Sci*, 33:215–245, January 2005.

[11] Mathew G. Wells and J. S. Wettlaufer. Circulation in lake vostok: A laboratory analogue study. *Geophysical research letters*, 30:501–505, February 2008.

[12] J. C. Mullarney G.O. Huges, R.W. Griffith and W.H. Peterson. A theoretical model for horizontal convection at high rayleigh number. *Journal of fluid mechanics*, 581:251–276, 2007.

[13] Graham O. Hughes and Ross W. Griffiths. Horizontal convection. *Annu. Rev. Fluid Mech.*, 40:185–208, 2008.

[14] G. O. Hughes B. Gayen, R.W. Griffiths† and J.A. Saenz. Energetics of horizontal convection. *J. Fluid Mech.*, 716:R10 1–11, February 2013.

[15] R.W. Griffiths J. Mullarney and O.G. Huges. Convection driven by differential heating at a horizontal boundary. *Journal of fluid mechanics*, 516:181–209, February 2004.

[16] Sheng-Qi Zhou Fei Wang, Shi-Di Huang and Ke-Qing Xia. Laboratory simulation of the geothermal heating effects on ocean overturning circulation. *Journal of Geophysical Research: Oceans*, 121:7589–7598, October 2016.

[17] J.W. Lottes P.F. Fischer and S.G. Kerkemeier. nek5000 web page. *Website, https://nek5000.mcs.anl.gov/*, 2008.

[18] P. Schlatter M. Andersson N. S. Abad, R. Vinuesa and M. Karlsson. Simulation strategies for the food and drug administration nozzle using nek5000. *AIP Advances*, February 2020.

[19] A.T. Patera. A spectral element method for fluid dynamics: laminar flow in a channel expansion. *Journal of Computational. Physics*, 54:468–488, June 1984.

[20] Jianzhao WU Zhiming LU Quan ZHOU Tianyong YANG, Bofu WANG. Horizontal convection in a rectangular enclosure driven by a linear temperature profile. *Applied Mathematics and Mechanics (English Edition)*, 021, June 2021.

[21] Siegfried Grossmann Guenter Ahlers and Detlef Lohse. Heat transfer large-scale dynamics in turbulent rayleigh-bénard convection. *Review of modern physics*, 81(2):503–537, April 2009.

[22] Irina Filina Malte Thoma, Klaus Grosfeld and Christoph Mayer. Modelling flow and accreted ice in subglacial lake concordia, antarctica. *Elsevier*, June 2009.

[23] Ross W. Griffiths Bishakhdatta Gayen and Graham O. Hughes. Stability transitions and turbulence in horizontal convection. *Journal of fluid mechanics*, 751:698–724, 2014.

Appendix

A Appendices

A.1 Reversals check

**Velocity fields superposed on time ave. mean flow speed**
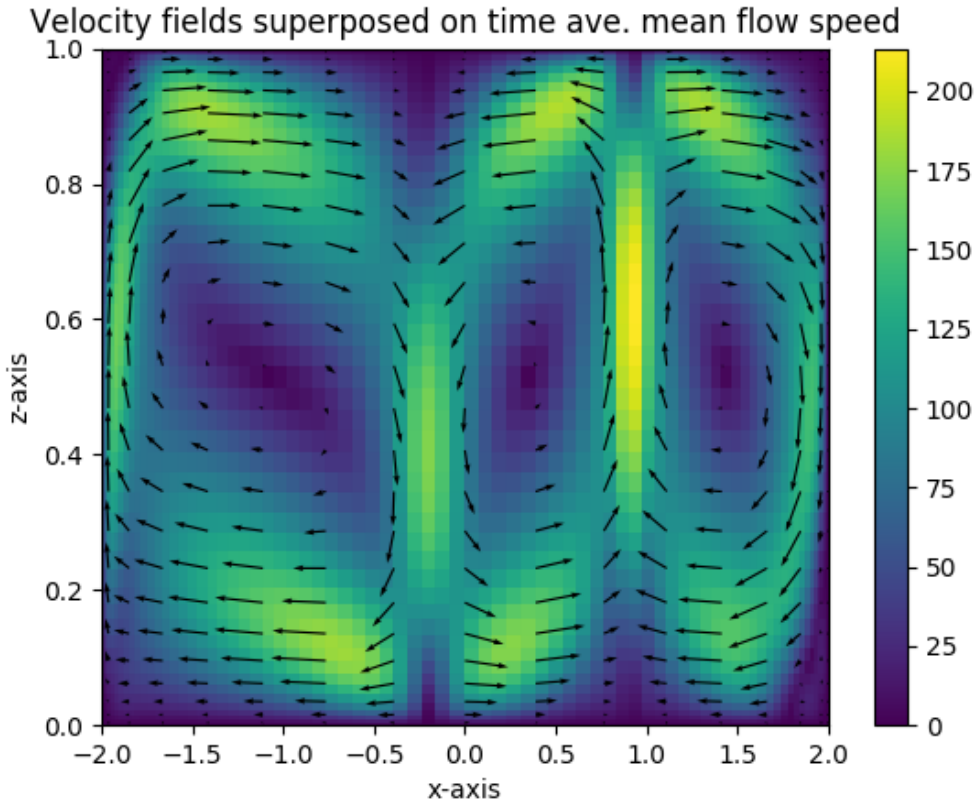
Figure 17: Time average mean flow plotted as a color mesh with vector fields superposed for $Ra = 10^6, hg = 0.001$ with an initial condition of zero temperature everywhere.

A.2 Aspect ratio 8

We use an aspect ratio of 8 such that our domain runs from $^-4H -^+ 4H$ along x-axis and $0 - H$ along z-axis. These results can be seen in figure 18. The first, second and third columns correspond respectively to hg=0, hg=0.001 and hg=0.01 where as the first, second and third rows are the results for the mean temperature, mean flow and convective flux respectively. Convective heat flux is computed by getting the product of vertical velocity,w and mean temperature,T, i.e., $ConvectiveFlux = wT$. Increasing the aspect ratio to 8 increases the width of the domain and creates more room for more cells and we count cell from 8 (hg=0) to 7 (hg=1) just like it was the case with aspect ratio 4 where we moved from 4 cells to 3.

A.3 Reynold's number
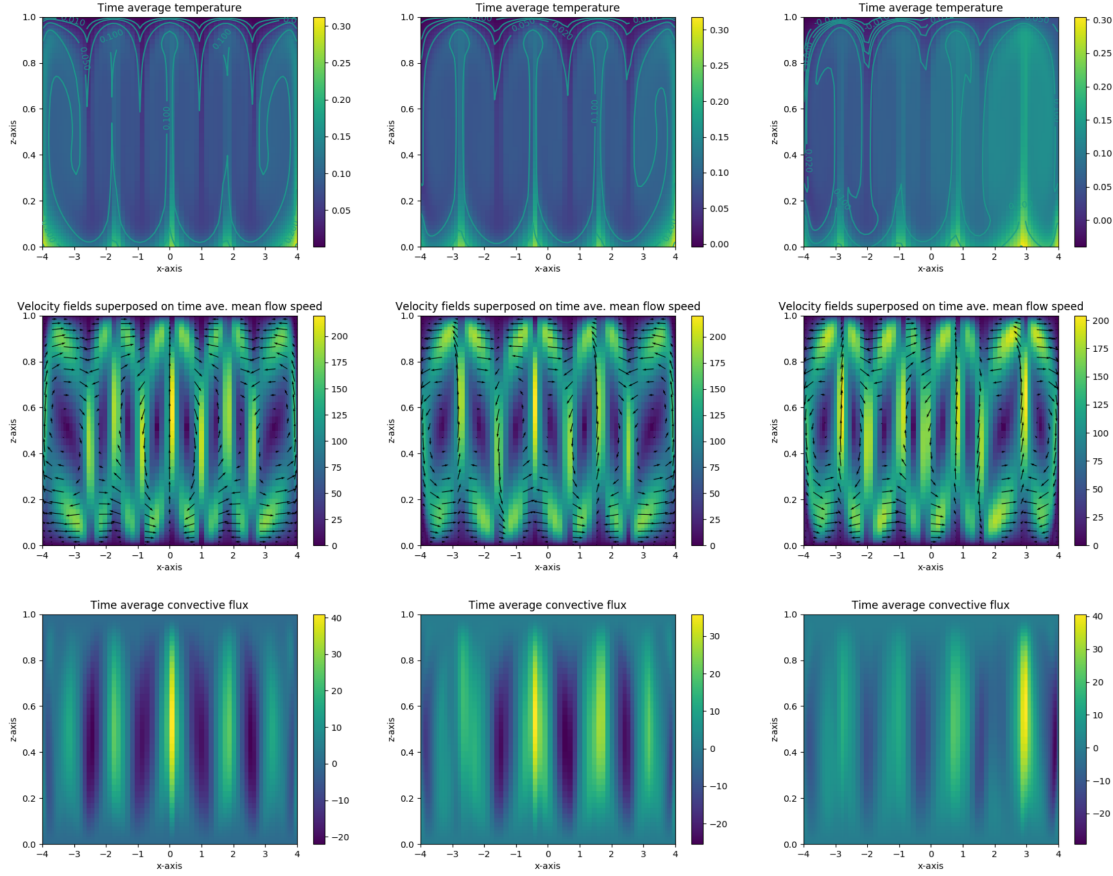
Figure 18: Simulations with Aspect ratio 8. The first, second and third columns are respectively hg=0,gh=0.001 and hg=0.01 where as the top, middle and bottom rows are results of mean temperature, mean flow and convective heat flux respectively.
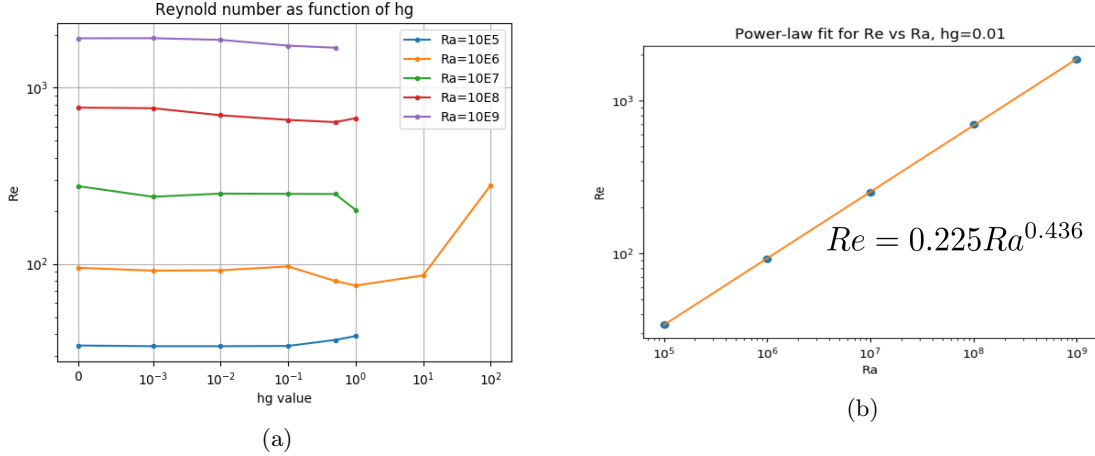
Figure 19: (a) Variation of Reynold's number with hg. Higher values of hg=10 and 100 are added to take into account fundamental fluid dynamics. For hg below 1.0, the Reynolds number does not vary much with increase in hg. However, for very high hg values greater than 1 (for example 10 and 100), Reynold's number should increase with increasing hg. The graph in figure 19a clearly verifies this. (b) is a graph of Power-law fit for Reynold's number versus Ra, hg=0.01. The dots represent the data points while the solid orange line shows the power-law fit.
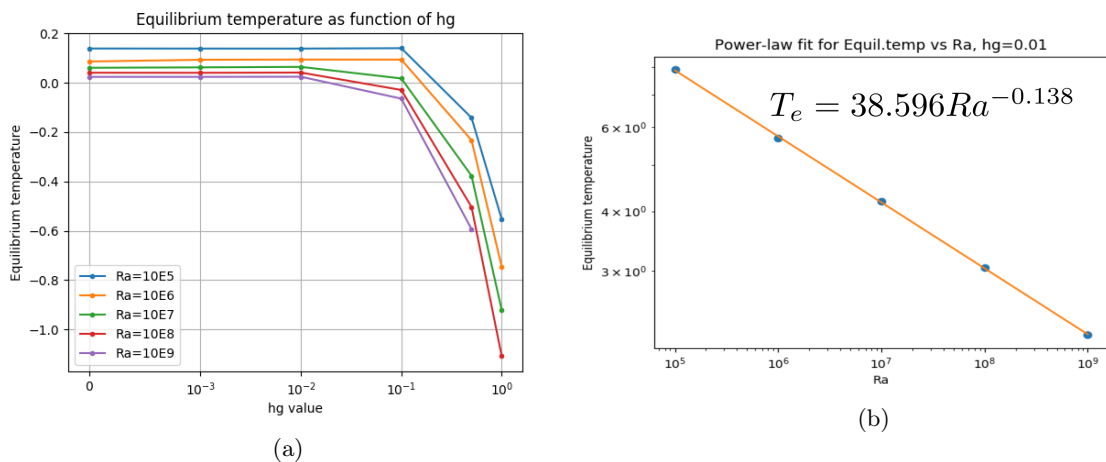

Figure 20: (a) Variation of equilibrium temperature (raw values-not corrected) with hg value. (b) A graph of Power-law fit for corrected normalised equilibrium temperature versus Ra, hg=0.01. The dots represent the data points while the solid orange line shows the power-law fit.
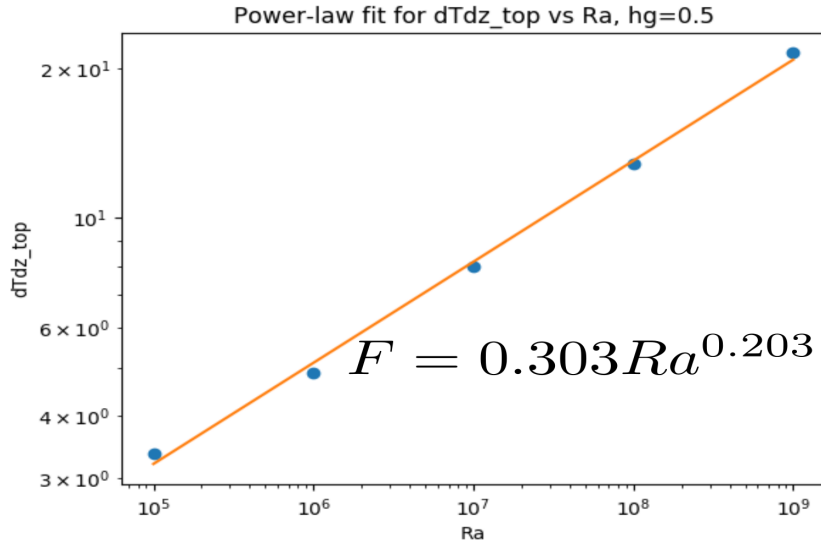
Figure 21: Power-law fit for top boundary flux versus Ra, hg=0.01.The dots represent the data points while the solid orange line shows the power-law fit.
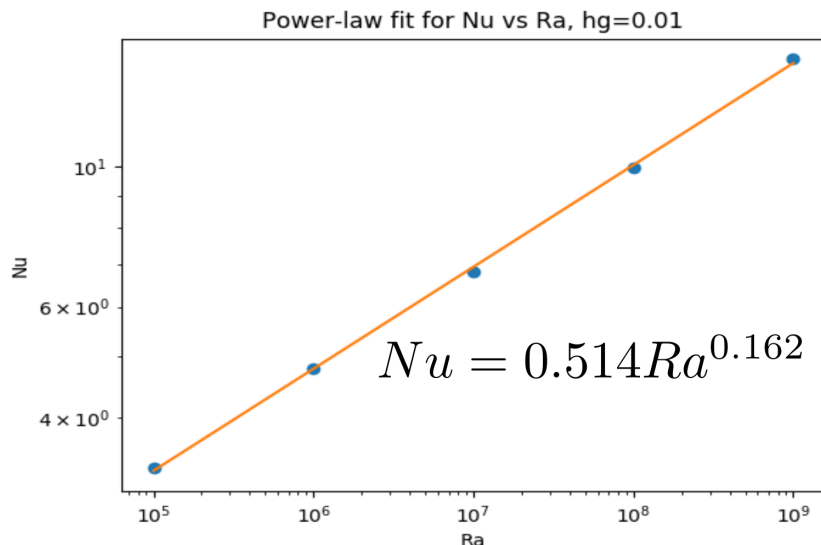

Figure 22: Power-law fit for Nu versus Ra, hg=0.01. The dots represent the data points while the solid orange line shows the power-law fit.
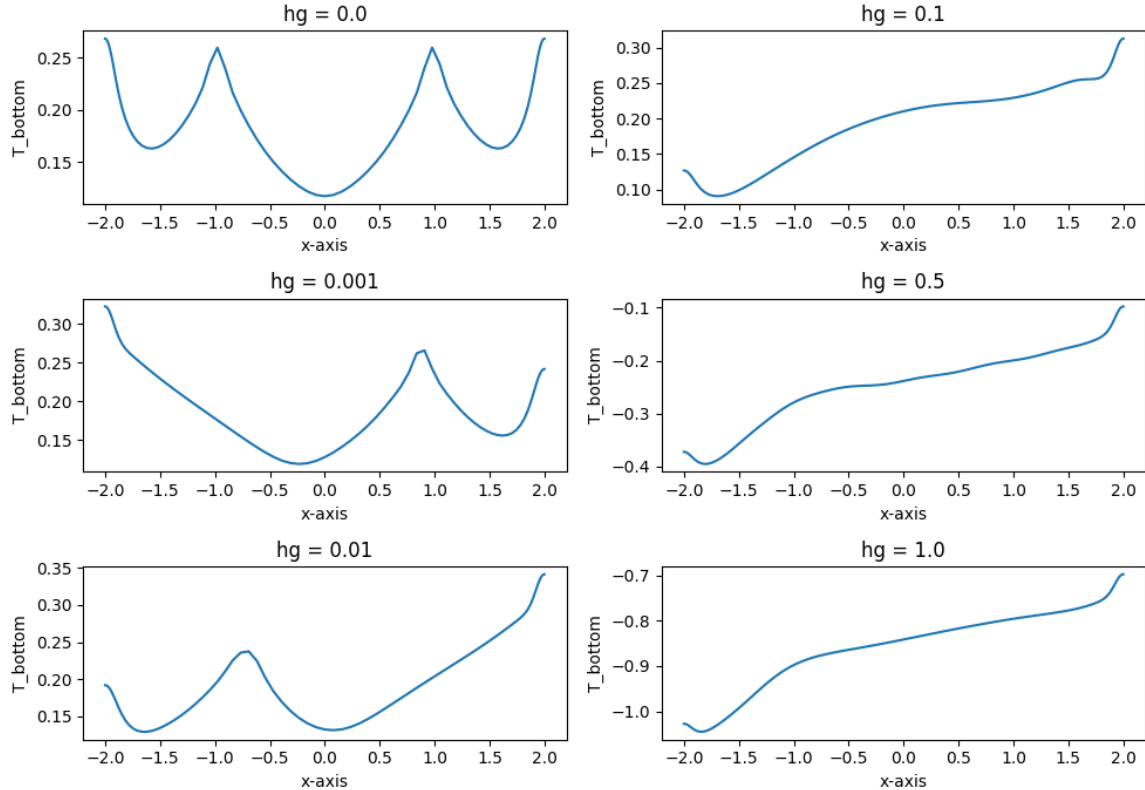
Figure 23: Time average bottom temperature at steady state for $Ra = 10^6$. When defining our problem, we imposed a flux at the bottom meaning the bottom temperature at the start is completely unknown. With a flux imposed at the bottom, this flux warms up the fluid; so the temperature of the fluid at the bottom boundary is expected to evolve with time. These plots thus demonstrate this time evolution of bottom temperature. We observe that the bottom temperature is always positive but with multiple maxima/minima for low hg values due to multiple RBC cells (Temperature values are minima where we expect a sinking plume and maxima where the plume is rising). Increasing hg values, bottom temperature is almost monotonously increasing left to right due to horizontal convection and downwelling for cold flows on the left for high hg.